Recent developments in the emerging field of crystalline p-type transparent conducting oxide thin films

A.N. Banerjee [a], K.K. Chattopadhyay [b,*]

[a] *Nanoscale Device Research, Department of Electrical & Computer Engineering, University of Nevada, Las Vegas, NV 89119, USA*
[b] *Thin Film and Nanoscience Laboratory, Department of Physics, Jadavpur University, Kolkata 700 032, India*

Abstract

Transparent, p-type semiconducting crystalline thin films have recently gained tremendous interest in the field of active devices. All-transparent junctional devices have begun a new generation in the optoelectronics technology called ''Invisible Electronics''. Non-stoichiometric and doped versions of various new types of p-type transparent conducting oxides (p-TCO) with improved optical and electrical properties have been synthesized in the last few years in this direction. A wide range of deposition techniques has been adopted to prepare the films. In this review we have tried to discuss the origin of p-type conductivity in these transparent oxides. Also an up-to-date and comprehensive description of different p-type transparent conducting oxide thin films is presented. The growth techniques of these films along with the relative deposition parameters are reviewed in detail. Electrical and optical properties of the films and fabrication of all-transparent diodes are discussed which are important in the development of ''Transparent Electronics''. Also, recently, the research on nanostructured materials generates great interest in the scientific community and offers tremendous opportunities in the field of physics, chemistry, materials science and related interdisciplinary areas because of new properties exhibited by them and challenging problems thrown up for providing theoretical concepts in physics associated with it. Here, we have also discussed in brief, the formation of different nanocrystalline p-TCO films, which may open up an extremely important and interesting field of research for the fabrication of all-transparent nanoactive devices and give a new dimension in the field of ''Transparent Electronics''.
© 2005 Elsevier Ltd. All rights reserved.

* Corresponding author. Tel.: +91 33 2867 1350.
  E-mail addresses: anb_2020@yahoo.co.in (A.N. Banerjee), kalyan_chattopadhyay@yahoo.com (K.K. Chattopadhyay).

1. Introduction

Transparent conducting oxides (TCO) are well known and have been widely used for a long time in optoelectronics industries as well as in research fields. The first report of transparent conducting thin films of cadmium oxide (CdO) was published in 1907 by Badekar [1] who prepared the films by thermal oxidation of sputtered films of cadmium. Since then extensive works have been done in the field of TCO technology to prepare new types of TCOs with wide ranging applications [2−12]. These well-known and widely used TCOs include SnO_2:Sb/F, ZnO:In/Al/F/B/Ga, In_2O_3:Sn/F/Sb/Pb, Cd_2SnO_4 etc. as well as some new TCOs such as Zn_2SnO_4, $ZnSnO_3$, $GaInO_3$:Ge/Sn, $AgInO_2$:Sn, $MgIn_2O_4$, $CdSb_2O_6$:Y, $Zn_2In_2O_5$, $ZnGa_2O_4$, $In_4Sn_3O_{12}$, $CdIn_2O_4$:Sn etc. [13−43]. As far as applications are concerned, TCOs are being used extensively in the window layers of solar cells, as front electrodes in flat panel displays (FPD), low-emissivity ("low-e") windows, electromagnetic shielding of cathode-ray tubes in video display terminals, as electrochromic (EC) materials in rear-view mirrors of automobiles, EC-windows for privacy (so-called "smart windows"), oven windows, touch-sensitive control panels, defrosting windows in refrigerators and airplanes, invisible security circuits, gas sensors, biosensors, organic light emitting diodes (OLED), polymer light emitting diodes (PLED), antistatic coatings, cold heat mirrors, etc. [1−4,8,9,13,44−54]. Also some new applications of TCOs have been proposed recently such as holographic recording media, high-refractive index waveguide overlays for sensors and telecommunication applications, write-once read-many-times memory chips (WORM), electronic ink etc. [55−58]. And lastly, the low-temperature deposition of TCOs onto poly(ethylene terephthalate) (PET), polyimides and other polymer substrates in roll-coating processes for touch-screen and infrared reflector applications are the recent challenges for the TCO industries [59,60].

Although the TCOs have a vast range of applications as mentioned above, very little work has been done on active device fabrication using TCOs [61,62]. This is because most of the aforementioned TCOs are n-type semiconductors. But the corresponding p-type transparent conducting oxides (p-TCO), which are essential for junction devices, were surprisingly missing in thin film form for a long time until in 1997, Kawazoe et al. from Tokyo Institute of Technology, Japan, reported p-type conductivity in a highly transparent thin film of copper aluminum oxide ($CuAlO_{2+x}$) [63]. This has opened up a new field in optoelectronics device technology, the so-called "Transparent Electronics" or "Invisible Electronics" [64], where a combination of the two types of TCOs in the form of a p−n junction could lead to a "functional" window, which transmits visible portion of solar radiation yet generates electricity by the absorption of the UV part [63]. It must be mentioned here that the first report of a semi-transparent p-type conducting thin film of nickel oxide (NiO) was published in 1993 by Sato et al. [65] from Kanazawa Institute of Technology, Japan. They observed about 40% transmittance of the NiO films in the visible region and when they tried to fabricate an all-TCO p−i−n diode of the form p-NiO/i-NiO/i-ZnO/n-ZnO, the visible transmittance further reduced to almost 20%. Although this low transmittance was not favorable for superior device applications, nevertheless the report was an important milestone in the field of "Transparent Electronics" and in the development of TCO technology.

The possibility of the above-mentioned novel applications of TCOs is based on the fact that the electronic bandgap of a TCO is higher than 3.1 eV (corresponding to the energy of a 400 nm blue photon). So visible photons (having energy between 2.1 and 3.1 eV) cannot excite electrons from valence band (VB) to the conduction band (CB) and hence are transmitted through it, whereas they have enough energy to excite electrons from donor level to CB (for

n-type TCO) or holes from acceptor level to VB (for p-type TCO) as described in Fig. 1. And these acceptor or donor levels are created in the TCOs by introducing non-stoichiometry and (or) appropriate dopants in a controlled manner.

Now for diverse device applications, it is of the utmost importance to prepare various new types of p-TCOs with superior optical and electrical characteristics, at least comparable to the existing, widely used n-TCOs, which have a transparency above 80% in the visible region and a conductivity of about 1000 S cm^{-1} or more. Intense works have been done for the last five years in this direction to fabricate new p-TCOs by various deposition techniques. Also quite a number of works have been carried out for proper understanding of the structural, optical and electrical characteristics of p-TCOs. As this is an emerging field in TCO technology, a systematic review of the major developments in p-TCO materials with regard to the different deposition techniques and properties of the films so obtained are the needs of the hour. A brief and partial review of this field had been reported previously by Tate et al. [66] as well as by Nagarajan et al. [67,68]. Also Norton [69] presented a detailed review on the synthesis and properties of oxide thin films, which briefly includes the importance of p-TCO too. Here we have tried to give a comprehensive and up-to-date picture of this interesting and challenging field of p-type transparent conducting oxides.

2. Criteria to choose p-TCO

Most of the existing TCOs are n-type, whereas it is very difficult to prepare binary metal oxides with p-type conductivity. A possible reason for this has been described by Kawazoe et al. [70], where they argued that this is probably because of the electronic structure of these metal oxides. Strong localization of holes (it can be successfully introduced by intentional substitutional doping or by producing non-stoichiometry within the material) at oxygen 2p levels or an upper edge of the valence band due to the high electronegative nature of oxygen, i.e. this localization is due to the ionicity of metallic oxides. O 2p levels are far lower lying than the valence orbit of metallic atoms [71], leading to the formation of a deep acceptor level by the holes. In other words, the holes therefore have high probability to be localized around the oxygen atoms. Hence these holes require high enough energy to overcome a large barrier height in order to migrate within the crystal lattice, resulting in poor conductivity and hole mobility.
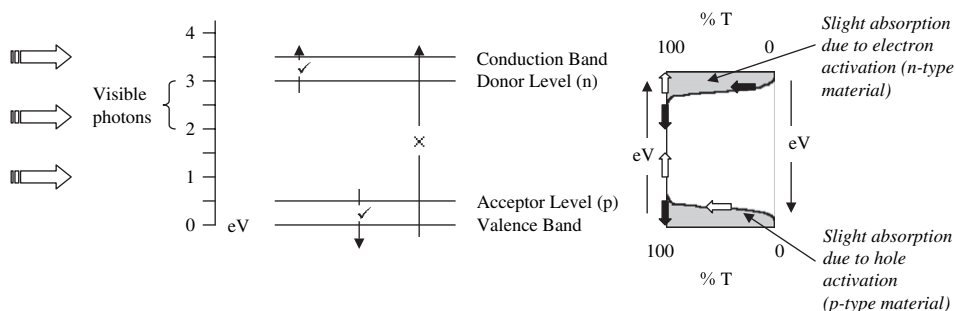

Fig. 1. Bandgap designing for transparent conductors. Visible photons (2.1−3.1 eV) do not have enough energy to excite electrons from valence band to conduction band, but have enough energy to excite holes (for p-type) from acceptor level to VB or electrons (for n-type) from donor level to CB.

A possible solution proposed by Kawazoe et al. [70] is to introduce a ''degree of covalency'' in the metal−oxygen bondings to induce the formation of an extended valence band structure, i.e. the valence band edge should be modified by mixing orbitals of appropriate counter cations that have energy-filled-levels comparable to the O 2p level. This would reduce the strong coulombic force by oxygen ions thereby delocalizing the holes. This is the essential approach to obtain p-TCO, which is called ''Chemical Modulation of the Valence Band (CMVB)'' [70].

But the next requirement is the choice of appropriate cationic species that will serve for the CMVB technique. Investigations showed that the required cationic species are the $3d^{10}$-closed shell of Cu^+ ions and $4d^{10}$-closed shell of Ag^+ ions [70,72]. Although some transition metal cations with an open d-shell may fulfill the energy requirement [73] for CMVB technique they usually show strong coloration due to a d−d transition, which is not expected for transparent materials. Hence the focus has been concentrated towards the cations mentioned above, with closed ($d^{10}s^0$) electronic configuration. Fig. 2 shows a schematic illustration of CMVB technique. Both of the atomic orbitals are occupied by electron pairs, and the resulting antibonding level becomes the highest occupied level, i.e. the valence band edge (as shown in Fig. 2).

Next is the structural requirement for designing p-TCO materials. Tetrahedral coordination of oxide ions is advantageous for p-type conductivity, as it acts in reducing the localization behavior of 2p electrons on oxide ions [70]. The valence state of the oxide ions can be expressed as sp^3 in this conformation. Eight electrons (including $2s^2$) on an oxide ion are distributed in the four σ bonds with the coordination cations. This electronic configuration reduces the non-bonding nature of the oxide ions and increases the delocalization of holes at the valence band edge (that is why Cu_2O is a p-type conducting oxide [74−77]). But Cu_2O, although p-type in nature, has rather small bandgap (2.17 eV) [75]. This is probably because of the three-dimensional interactions between $3d^{10}$ electrons of neighboring Cu^+ ions. It is expected that the low-dimensional crystal structure would suppress this interaction [78]. As we are interested in transparent conducting oxides, the bandgap of the material (E_g) should be greater than 3.1 eV. Hence enlargement of bandgap would be another structural requirement for designing p-TCO, so that there is no absorption of visible photons. Materials with delafossite crystal structure $M^IM^{III}O_2$ (M^I = monovalent ions, Cu^+, Ag^+; M^{III} = trivalent ions, Al^{+3}, Ga^{+3}, In^{+3}, Cr^{+3}, Fe^{+3}, Co^{+3} etc.) [79−81] were chosen as the candidates for p-TCOs for several reasons. First, if we investigate the delafossite structure as shown in Fig. 3, we see an
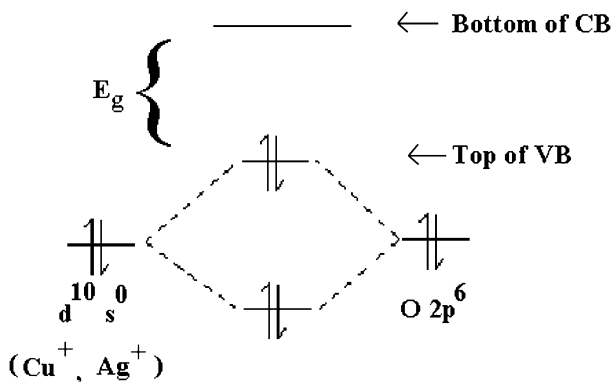

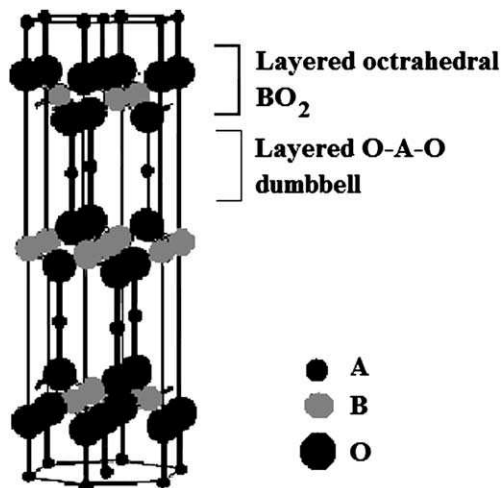Fig. 2. Schematic diagram of CMVB method (after Ref. [70]).

Fig. 3. Delafossite crystal structure (after Ref. [190]).

alternative stacking of M^I and layers of nominal $M^{III}O_2$ composition consisting of $M^{III}-O_6$ octahedra sharing edges. Each M^I atom is linearly coordinated with two oxygen atoms to form an $O-M^I-O$ dumbbell unit placed parallel to the c-axis. O-atoms of $O-M^I-O$ dumbbell link all M^I layers with the $M^{III}O_2$ layers. On the other hand each oxide ion in the $M^{III}O_2$ layer forms a "pseudo-tetrahedral coordination $(M_3^{III}M^IO)$" [70] with the neighboring M^{III} and M^I ions. Hence, as previously mentioned this electronic configuration reduces the non-bonding nature of the oxide ions and therefore delocalizes the holes at the valence band edge. Second, this layered structure ($O-M^I-O$ dumbbell layer and $M^{III}O_2$ layer) effectively reduces the dimension of crosslinking of M^I ions thus enlarging the bandgap [63]. And finally, another important factor in this structure is the low coordination number of the M^I ions, due to the large separation from oxygen ligands, which is the result of the strong coulombic repulsion between 2p electrons in oxygen ligands and M^I d^{10} electrons. This leads to the M^I d^{10} energy levels almost comparable to the O 2p level, resulting in a high degree of mixing of these levels, which is essential for the CMVB technique [70].

As the importance of p-TCO lies in the active device fabrication, it is very important to have lattice matching between both the p and n-types of the TCOs to form p−n homo-junctions. Both types of TCOs with delafossite structure may serve this requirement. In this regard, it is also worthwhile to mention that the $M^{III}O_2$ layers of this structure is also important for designing n-TCOs, specially for the cations like Ga^{+3}, In^{+3} in the M^{III} sites with s^0 configuration [70]. Following the above argument, a delafossite $AgInO_2$ thin film with n-type semiconductivity has already been demonstrated [36].

3. p-Type transparent conducting oxides with delafossite structure

3.1. $CuM^{III}O_2$ (M^{III} = trivalent cations)

The first and the most important material in this group is copper aluminum oxide ($CuAlO_2$). This material has been known to exist for nearly 50 years [82]. Back in 1984 its p-type

conductivity was first reported by Benko and Koffyberg [83], although Kawazoe et al. [63] first prepared it in transparent thin film form for possible application in p-TCO technology. The structural properties of this material were extensively studied by Ishiguro et al. [84−86]. The structure is shown in Fig. 3. It belongs to the $R\bar{3}m$ (D_{3d}) space group with rhombohedral crystal structure [84]. Other p-TCO thin films belonging to this group are copper gallium oxide ($CuGaO_2$) and copper indium oxide ($CuInO_2$) [87−89]. The lattice parameters of these materials were reported in various literatures [80,83,90,91]. Also, the band structures of these materials were calculated by Yanagi et al. [78], Robertson et al. [92] and in detail by Ingram et al. [93].

Doped versions of some similar types of p-TCO thin films have also been reported which include iron doped copper gallium oxide ($CuGaO_2$:Fe), calcium doped copper indium oxide ($CuInO_2$:Ca), magnesium doped copper scandium oxide ($CuScO_2$:Mg), magnesium doped copper chromium oxide ($CuCrO_2$:Mg), calcium doped copper yttrium oxide ($CuYO_2$:Ca) etc. [66,88,89,94−96]. Crystallographic data as well as band structure calculations of these materials had also been reported in various literatures [90,97,98]. Preparation of some other highly resistive ($\sim 10^6$ Ω cm) new delafossite materials such as $CuFe_{1−x}V_xO_2$ ($x = 0.5$), $CuNi_{1−x}Sb_xO_2$, $CuZn_{1−x}Sb_xO_2$, $CuCo_{1−x}Sb_xO_2$, $CuMg_{1−x}Sb_xO_2$, $CuMn_{1−x}Sb_xO_2$ ($x = 0.33$) in powder form had been reported by Nagarajan et al. [67,68] (but no thin film preparation of these materials has been reported so far). Preparation of 10% Sn doped $CuNi_{1−x}Sb_xO_2$ thin film has been reported by the same group [66,68], having reasonable visible transparency (60%) and conductivity (5×10^{-2} S cm^{-1}).

3.2. $AgM^{III}O_2$ (M^{III} = trivalent cations)

Most of the p-type semiconducting delafossite materials are Cu based. Corresponding Ag-based delafossite materials are difficult to be synthesized by simple solid-state reaction [66]. The first report of Ag-based delafossite thin film was $AgInO_2$, which is n-type in nature [36]. Later, Nagarajan et al. [67] reported that Mg-doped $AgInO_2$ powder ($AgIn_{1−x}Mg_xO_2$, $x = 0.1$), when treated with fluorine or high-pressure oxygen developed a p-type nature whose conductivity was observed to be as low as 10^{-6} S cm^{-1}. A series of similar types of delafossite materials have been synthesized by the same group [67], but only in powder form; they include $AgScO_2$, $AgCrO_2$, $AgGaO_2$ etc. All of these pellets showed very low conductivity ($\sim 10^{-6}$ S cm^{-1}) and no thin film preparations of these materials have been reported so far. On the other hand, the first report of Ag-based delafossite thin film with p-type conductivity was reported by Tate et al. [66], which is silver cobalt oxide (Ag_xCoO_2; $x < 1$). The film showed reasonable conductivity (2×10^{-1} S cm^{-1}) and almost 50% transparency in the visible region with a direct bandgap value of 4.15 eV (shown in Fig. 4(a) and (b)). The better conductivity of this film over other Ag-based delafossite materials may be attributed to the greater degree of mixing between Co 3d^{10} orbitals and O 2p^6 orbitals, resulting in larger delocalization of holes [99,100]. Doped versions of some other Ag-based delafossites have also been reported such as $AgNi_{1−x}Sb_xO_2$, $AgZn_{1−x}Sb_xO_2$ ($x = 0.33$) etc. [66] but only in powder form. Also no comments on the nature of conductivity of these powders were given in the literature.

Regarding relative comparison between Cu-based delafossites and Ag-based delafossites, it has been suggested [101] that the former group should be better candidates as transparent conductors because of their greater hole mobility, which is due to the Cu-3d character of the valence band edge of Cu-based delafossites. Whereas for Ag-based delafossites, the valence band edge possesses O-2p character and d-manifold holes are more mobile than that of p-manifold [67].
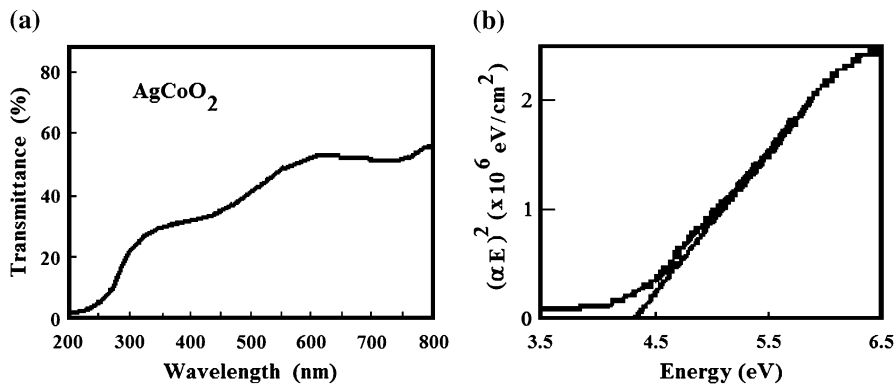
(a)   **(b)**

Fig. 4. (a) Optical transmission of an AgCoO$_2$ thin film (after Ref. [66]). (b) Determination of direct bandgap of an AgCoO$_2$ thin film (after Ref. [66]).

3.3. Non-stoichiometry and doping in delafossite p-TCO thin films

The cause of p-type conductivity shown by these types of materials is due to excess oxygen (or metal deficit) within the crystallite sites of the material i.e. the defect chemistry plays an important role. This deviation from the stoichiometric composition of the components can be induced by regulating the preparation condition of the materials. The defect reaction may be represented by the following equation [102,103]:

$$O_2(g) = 2O_O^x + V_{M^I}^- + V_{M^{III}}^{-3} + 4h^+ \tag{1}$$

where "O_O" denotes the lattice oxygen, "V" s denote the vacancies of monovalent cation M^I and trivalent cation M^{III}, respectively, and "h" denotes the hole. Superscripts x, $-$, and $+$ denote effective neutral, negative, and positive charge states, respectively.

Also, intercalation of excess O^{-2} ions in the interstitial sites may trap electrons, leaving behind empty states in the valence band, which act as holes. The formula for oxygen-excess delafossite films may be written as $M^I M^{III} O_{2+x}$ ($M^I = Cu^+$, Ag^+ and $M^{III} = Al^{+3}$, Ga^{+3}, In^{+3}, Y^{+3}, Sc^{+3} cations etc.). The value of x i.e. the percentage of excess oxygen may be as low as 0.001% in CuAlO$_{2+x}$ thin film [64] to more than 25% in CuYO$_{2+x}$ polycrystalline powder and CuScO$_{2+x}$ thin films [67,104−106]. Fig. 5(a)−(c) shows schematic representation of stoichiometric ABO$_2$ crystal and non-stoichiometric ABO$_2$ crystal with "excess" oxygen in lattice sites and interstitial sites. Figs. 6−8 show some experimental evidence in support of the theory of enhanced p-type conductivity due to excess oxygen.

Oxygen intercalation in delafossite p-TCOs only showed a maximum reported conductivity around 3×10^1 S cm^{-1} [94]. But this is still quite smaller than that of commercially available n-TCOs like indium tin oxide (ITO), which has a room-temperature conductivity of more than 1×10^3 S cm^{-1}. So the next activity was focused on the substitutional doping of these materials by appropriate dopants in order to increase their conductivity. Doping of CuAlO$_2$ was attempted first, as it was the first reported material amongst the p-TCOs. Several groups theoretically calculated the effects on the electronic behavior of the material due to the presence of various cations in Cu and (or) Al sites. Lalić et al. [107,108] showed that Cd and Zn substitutions on Cu site would produce n-type conductivity in the material, whereas Ni doping in Cu sites would
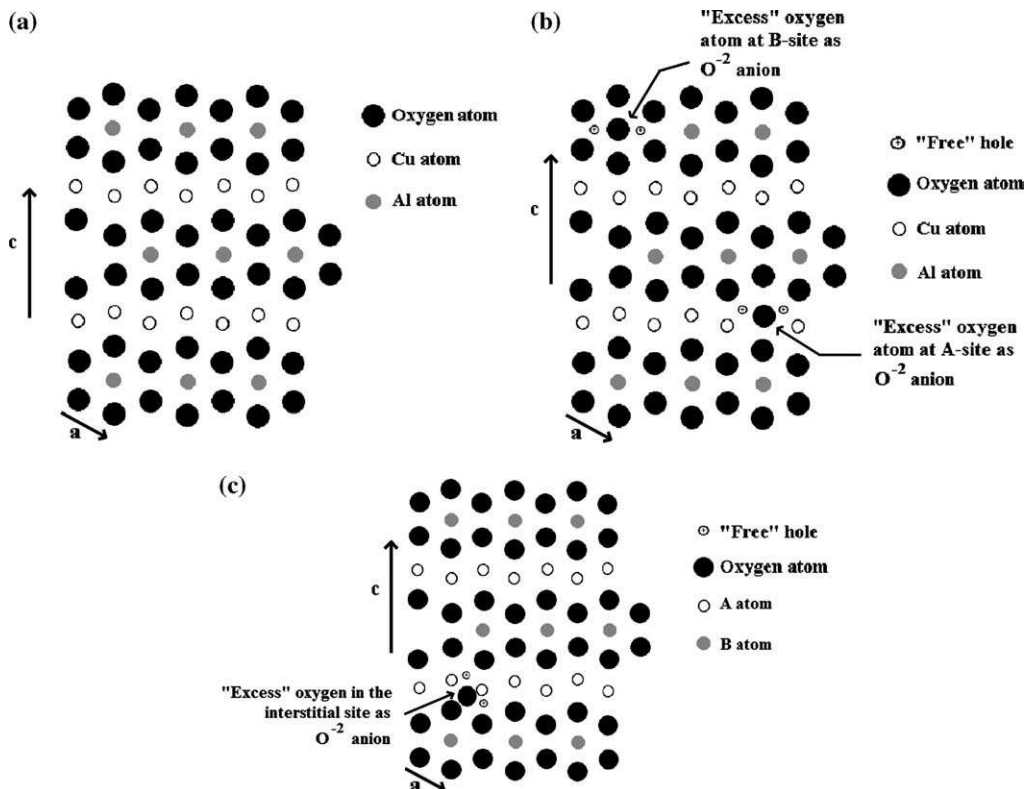
Fig. 5. (a) Stoichiometric ABO_2 lattice. (b) Non-stoichiometric ABO_2 indicating excess oxygen in A-lattice site and B-lattice site. Four holes are created making the material p-type conducting. (c) Non-stoichiometric ABO_2 lattice indicating excess oxygen in interstitial sites. Each interstitial oxygen traps electrons to form an O^{-2} anion, leaving behind two holes (after Ref. [181]).

enhance the p-type conductivity of the material. But Cd doping on Al sites would have no effect on the electrical properties of the material.

Preparation of a solid solution of gallium doped copper aluminum oxide in the form of $CuAl_{1-x}Ga_xO_2$ ($0 \leq x \leq 0.5$) was reported by Shahriari et al. [109]. But no film preparation of this material was reported by them. Also no other experimental data on the doping of $CuAlO_2$ thin film have so far been reported.

Heavy doping ($\sim 50\%$) of $CuGaO_2$ by Fe^{+3} in Ga sites has been reported by Tate et al. [66]. Their strategy was to combine high transparency of $CuGaO_2$ thin film ($\sim 80\%$ in the visible region [87]) with better conductivity (over other Cu and Ag-based delafossites [81]) of $CuFeO_2$ pellets (2.0 S cm^{-1} [81,110]).

Both the polycrystalline powder and thin film of $CuGa_{1-x}Fe_xO_2$ ($0 \leq x \leq 1$) have shown p-type conductivity. It was observed that high Fe doping increased the conductivity of the film from 2×10^{-2} S cm^{-1} (for an undoped $CuGaO_2$ thin film) to almost 1.0 S cm^{-1} for a $CuGa_{1-x}Fe_xO_2$ ($x = 0.5$) thin film, whereas transparency of the films became $\sim 60\%$ in the visible region [66]. The temperature variations of conductivity of undoped and Fe-doped $CuGaO_2$ thin films are shown in Fig. 9. Doping of $CuInO_2$, $CuYO_2$, $CuScO_2$, $CuCrO_2$ by divalent cations e.g. Ca^{+2}, Mg^{+2} etc. were reported by various groups [66,67,88,89,94−96]. When a trivalent cation
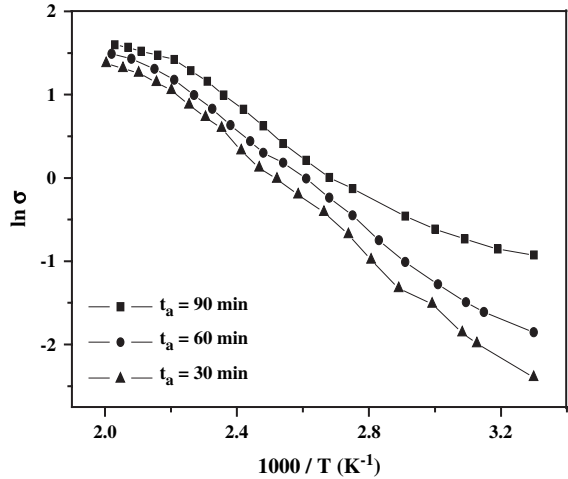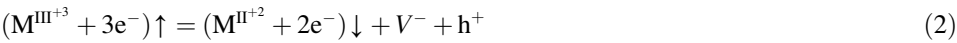
Fig. 6. Increase in the conductivity of CuAlO$_2$ thin film with increase in post-deposition oxygen annealing time (t_a), indicating the presence of excess (non-stoichiometric) oxygen in the lattice sites and (or) interstitial sites to enhance p-type conductivity (after Ref. [197]).

was replaced by a divalent cation, one empty state in the valence band was created, which acted as a hole, thus increasing hole conductivity. The method may be described by the following equation:

$$(M^{III^{+3}} + 3e^-)\uparrow = (M^{II^{+2}} + 2e^-)\downarrow + V^- + h^+ \tag{2}$$

where $M^{III^{+3}}$ and $M^{II^{+2}}$ are trivalent and divalent cations, V^- is the empty state, which is occupied by an electron, e^- and thus creating a "free" hole, h^+. The symbols $\uparrow$ and $\downarrow$ denote the replacement of the trivalent cation by a divalent one in the lattice sites. Such doped delafossite
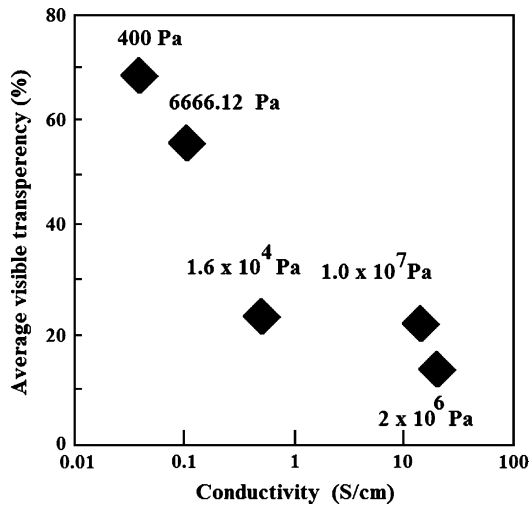

Fig. 7. Evidence for the increase in conductivity of CuScO$_{2+x}$:Mg thin films for different post-annealing O$_2$ pressure. An increase in conductivity leads to a decrease in the transparency of the films (after Ref. [66]).
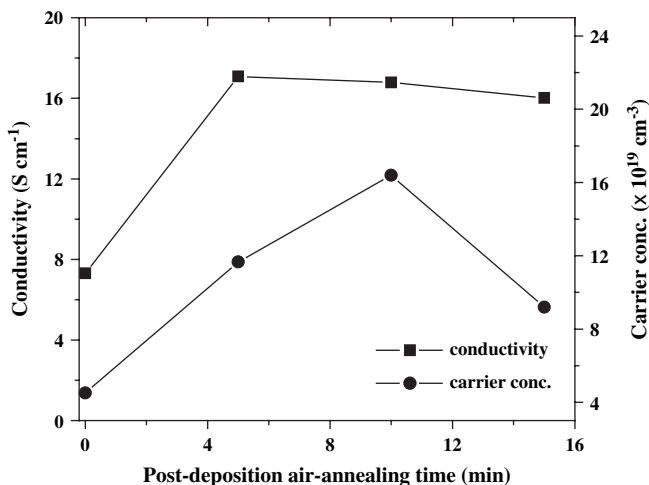
Fig. 8. Increase in conductivity of Cu−Al−O thin films with increase in annealing time. Evidence in support of enhanced p-type conduction due to excess oxygen (after Ref. [182]).

films like $CuCr_{1-x}Mg_xO_2$ ($x = 0.05$), $CuY_{1-x}Ca_xO_2$ ($x = 0.01-0.02$), $CuSc_{1-x}Mg_xO_2$ ($x = 0.05$) showed better hole conductivity (shown in Fig. 10) over the corresponding undoped films. The electrical and optical properties of these films are described in Table 1. Many types of material are yet to be explored completely. Tremendous opportunities are there to carry out intense research work in this field.

Some Ag-based delafossite materials like $AgM^{III}O_2$ ($M^{III} = Sc^{+3}$, Cr^{+3}, Ga^{+3} etc.) with 5% Mg doping at M^{III} sites were reported by Nagarajan et al. [67]. The conductivities of these
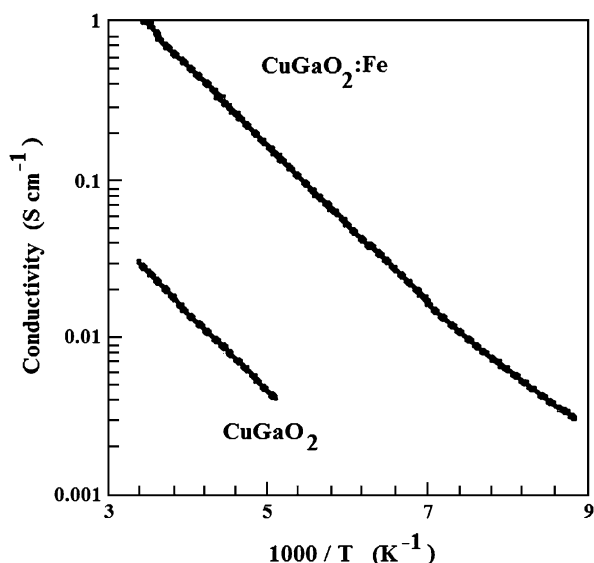

Fig. 9. Temperature dependence of conductivity of undoped and Fe-doped delafossite $CuGaO_2$ thin films, indicating increase in conductivity with doping (after Ref. [66]).
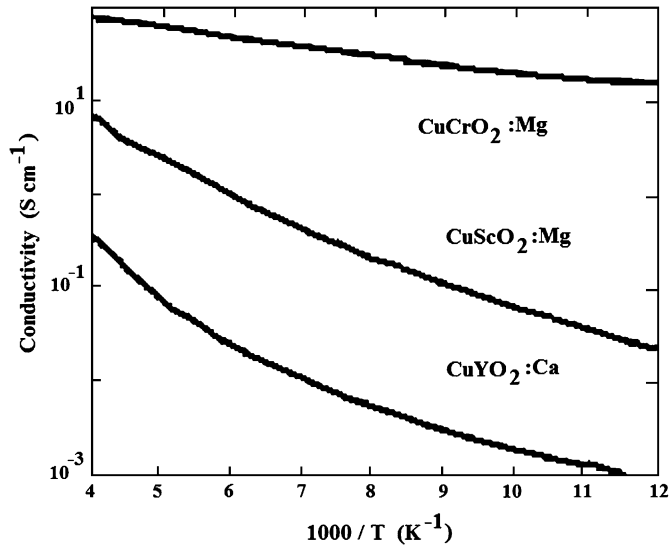
Fig. 10. Temperature dependence of conductivity of some doped delafossite thin films (after Ref. [95]).

sintered powders were very low ($\sim 10^{-5}$–10^{-4} S cm^{-1}) and also no film preparation of these materials have been reported anywhere so far.

There are also reports in the literature about the double substitution of trivalent M^{III} sites by divalent and pentavalent cations e.g. $CuFe_{1-x}V_xO_2$ ($x = 0.5$), $CuNi_{1-x}Sb_xO_2$, $CuZn_{1-x}Sb_xO_2$,

Table 1
Delafossite p-TCO thin films with different doping concentrations and their respective optoelectrical parameters

Material	Dopant	% of doping	Average film thickness (nm)	T (%)	$E_{g\text{-direct}}$ (eV)	σ_{RT} (S cm^{-1})	S_{RT} (μV K^{-1})	Reference
CuAlO$_2$	Undoped	–	230	70	3.5	0.34	+214	78
CuGaO$_2$	Undoped	–	500	80	3.6	0.063	+560	87
CuGa$_{1-x}$Fe$_x$O$_2$	Fe	0.5	150	60	3.4	1.0	+500	66
CuIn$_{1-x}$Ca$_x$O$_2$	Ca	0.07	170	70	$\sim$3.9	0.028	+480	88
CuCrO$_2$	Undoped	–	250	40	$\sim$3.1	1.0	–	95
CuCr$_{1-x}$Mg$_x$O$_2$	Mg	0.5	270	50	3.1	220	+150	95,67
CuYO$_2$	Undoped	–	200	60	$\sim$3.5	0.025	–	96,67
CuY$_{1-x}$Ca$_x$O$_2$	Ca	0.01–0.02	240	50	3.5	1.05	+275	96,67
CuScO$_2$[a]	Undoped	–	110	40	$\sim$3.3	30.0	–	94,67
CuSc$_{1-x}$Mg$_x$O$_2$[b]	Mg	0.05	220–250	80	3.3–3.6	$\sim$0.07	–	66,111
				60	-do-	$\sim$0.1	–	
				25	-do-	$\sim$0.8	–	
				15	-do-	$\sim$20.0	–	
CuNi$_{1-x}$Sb$_x$Sn$_y$O$_2$	Ni	0.66	$\sim$200	60	3.4	0.05	+250	66
	Sb	0.33						
	Sn	0.033						
AgCoO$_2$[c]	Undoped	–	150	50	4.15	0.2	+220	66

[a] Maximum of 25% oxygen was intercalated.
[b] The variation of transparency of the films at the expense of conductivity was due to a variation of oxygen pressure from 3 Torr (for most transparent film) to 15,000 Torr (for least transparent film). Also according to Ref. [111] the doping concentration of Mg was 1%.
[c] The Ag:Co ratio was 1.1:1.

CuCo$_{1-x}$Sb$_x$O$_2$, CuMg$_{1-x}$Sb$_x$O$_2$, CuMn$_{1-x}$Sb$_x$O$_2$ ($x = 0.33$), AgNi$_{1-x}$Sb$_x$O$_2$, AgZn$_{1-x}$Sb$_x$O$_2$ ($x = 0.33$) etc., but all in the form of sintered powder [67,68]. Also triple substitution of trivalent cations had been reported by Tate et al. [66,68] in the form of CuNi$_{1-x}$Sb$_x$Sn$_y$O$_2$ ($x = 0.3$, $y = 0.033$). Thin films of this material showed an average of 60% transmittance with a room-temperature conductivity of 5×10^{-2} S cm^{-1}. All the electro-optical parameters as well as doping concentrations of the above-mentioned materials only in thin film form have been furnished in Table 1.

4. Non-delafossite p-type transparent conducting oxides

4.1. Cu$_2$SrO$_2$

Besides delafossite films, another type of p-TCO thin film in the form of Cu$_2$SrO$_2$ has been synthesized by Kudo et al. [112]. The crystallographic data and band structure calculations were done by Teske and Müller-Buschbaum [113], Boudin et al. [114] and Robertson et al. [92]. This material has a body-centered tetragonal crystal structure with an $I4_1/amd$ (D_{4h}^{10}) space group. Its structure (shown in Fig. 11) has O−Cu−O dumbbells in the form of one-dimensional zigzag chains and separated by SrO$_6$ octahedra. This structure restricted the Cu−Cu interaction between the nearest neighboring d^{10} electrons to a single chain. This dimensional reduction of Cu−Cu interaction was proposed in order to increase the bandgap [112], which is essential for transparent materials. Undoped and 3% K-doped films were prepared by Kudo et al. [112]. The transparency of the films remain almost same ($\sim 70\%$ to 75%) for both types of films whereas the conductivity increased slightly from 3.9×10^{-3} S cm^{-1} for undoped films to 4.8×10^{-2} S cm^{-1} for K-doped films (shown in Figs. 12 and 13). Table 2 shows the different electrical and optical parameters of these films.

4.2. Spinel oxide films

Spinel films (the structure is of general formula AB$_2$O$_4$) of cobalt nickel oxide (NiCo$_2$O$_4$) with p-type conductivity and reasonable visible transparency ($\sim 40\%$ to 60%) have been
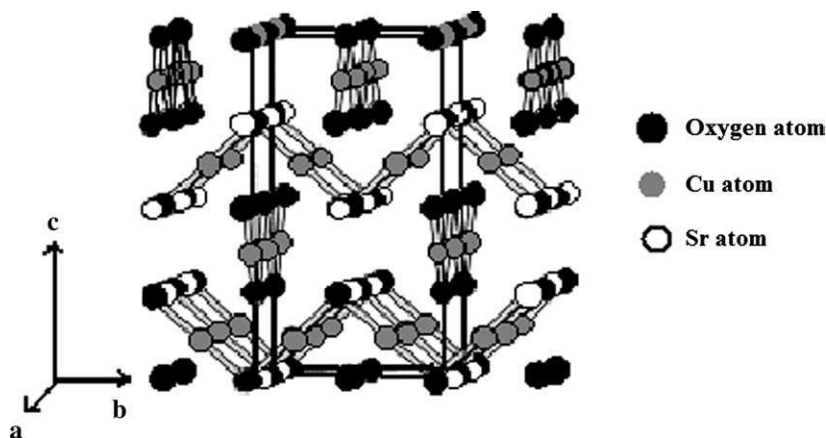

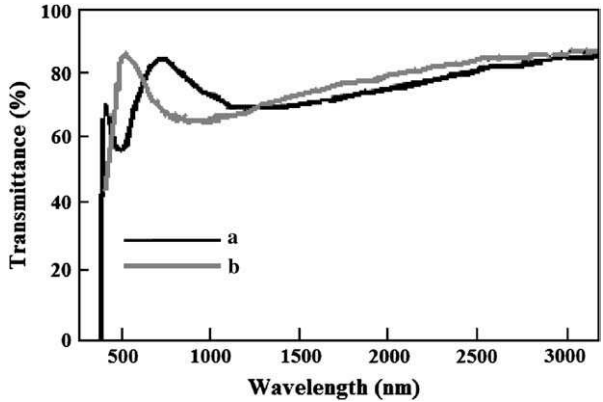Fig. 11. Crystal structure of SrCu$_2$O$_2$ (after Ref. [114]).

Fig. 12. Transmission spectra of (a) undoped, and (b) K-doped $SrCu_2O_2$ thin film (after Ref. [112]).

synthesized by Windisch et al. [115]. They observed a variation in the conductivity with a change in the Ni:Co ratio in the film and at Ni:Co = 1:2, the highest conductivity in these films was observed ($\sim 16\ S\ cm^{-1}$). They proposed that Ni^{+3} ions located on octahedral sites within the spinel lattice enhance the conductivity of the film [116]. Fig. 14 shows the variation of resistivity of Ni–Co–O thin films with composition x (= Co/{Co + Ni}). Minimum resistivity was obtained at $x = 0.67$. These films also showed good transparency in the infrared region, extending its application into infrared optics [115,117].

4.3. Layered oxychalcogenide films

Layered-structure oxychalcogenide films of the form $(LaO)CuC^h$ (C^h = chalcogenides e.g. S, Se) showed high optical transparency and reasonable p-type conductivity to become promising material for "Transparent Electronics" [118,119]. Although this material was first prepared almost two decades ago by Palazzi [120] its p-type conductivity was reported more
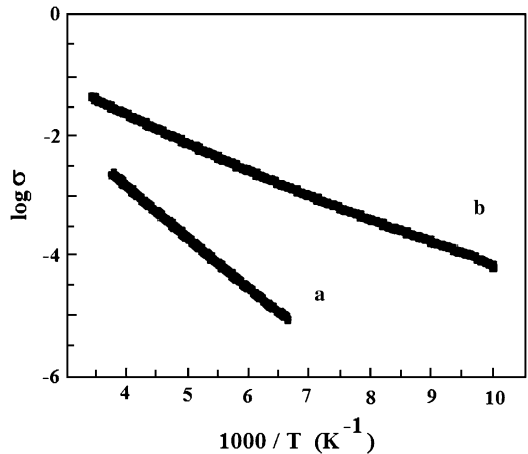

Fig. 13. Temperature variation of conductivity (σ) of (a) undoped, (b) K-doped $SrCu_2O_2$ thin films (after Ref. [112]).

Table 2

Non-delafossite p-TCO thin films with different doping concentrations and their respective optoelectrical parameters

Material	Dopant	% of doping	Average film thickness (nm)	T (%)	$E_{\text{g-direct}}$ (eV)	σ_{RT} (S cm^{-1})	S_{RT} (µV K^{-1})	Reference
Cu_2SrO_2	Undoped	−	150	75	∼3.3	0.004	260	112
$Cu_2Sr_{1-x}K_xO_2$	K	0.03	120	75	∼3.25	0.05	260	112
$NiCo_2O_4$	Undoped	−	100	∼65	−	∼16.67	−	115
$(LaO)CuS$	Undoped	−	150	70	∼3.1	6.4×10^{-5}	713	119
$(La_{1-x}Sr_xO)CuS$	Sr	0.03	150	60	∼3.1	20	44	119
$(LaO)CuS_{1-x}Se_x$	Se	0.0	∼150	∼60	>3.1	∼0.6	∼250	128
		0.25				∼2.5	∼200	
		0.4				∼20	∼250	
		0.7				∼15	∼150	
		1.0				∼25	∼250	
$(La_{1-x}Mg_xO)CuSe$	Mg	0.0	∼150	−	−	24	−	128
		0.2				140[a]	−	
$In_2O_3−Ag_2O$[b]	−	−	300	∼20	−	100	−	137
NiO[c]	Undoped	−	111	40	∼3.8	7.0	−	65
p-ZnO	Ga and N co-doped [d]	−	−	∼90	−	0.23	−	164

[a] The film showed degenerate p-type semiconductivity.
[b] The film contained 50 wt% Ag_2O.
[c] Data given for the films deposited under an atmosphere of Ar + 50 vol% O_2.
[d] N:Ga ratio was 2:1 with 5 wt% co-doped Ga in the film.

than a decade ago [121,122]. Ueda, Hiramatsu and co-authors first prepared it in transparent thin film form to extend its application into p-TCO technology [118,119]. Also this material shows room-temperature band edge emission under UV-excitation, extending its application in light emitting devices (LEDs) and similar fields [123−129]. Crystallographic parameters
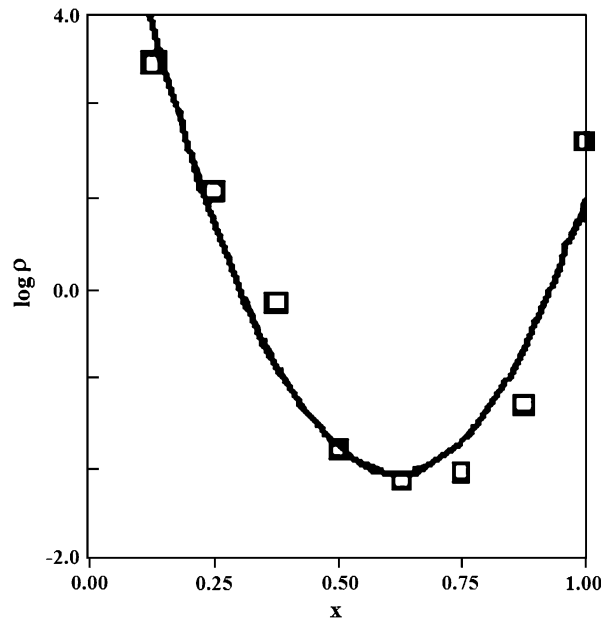

Fig. 14. Variation of resistivity of Ni−Co−O thin films with composition x ($= $Co/{Co + Ni}). Minimum resistivity obtained at $x = 0.67$ (after Ref. [115]).
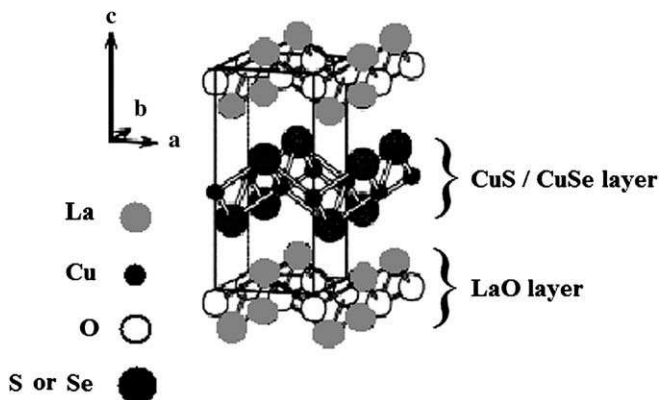
Fig. 15. Crystal structure of (LaO)CuC^h (C^h = S/Se) (after Ref. [124]).

of these materials were extensively studied by Palazzi [120] as well as by others [121,130,131]. Also band structure calculations were done by Inoue et al. [132]. Different physical properties of the material were also studied by various groups [133–135]. (LaO)CuC^h (C^h = S/Se) have tetragonal crystal structure with $P4/nmm$ space group [120,121] (crystal structure is shown in Fig. 15). The CMVB technique [70] adopted for designing p-type TCOs was successfully extended to these types of materials also, as described by Ueda et al. [118]. The S 3p and Se 4p orbitals are lower lying than O 2p orbitals. This widens the bandgap, keeping the material transparent in the visible region. Similarly, a high-energy shifting of the conduction band edge occurs in the material due to the presence of highly electropositive rare-earth material like La. This also reduces the number of Cu–S bonds in a unit cell, thus producing band dispersion at the valence band edge and hence enhances the hole mobility [118]. Undoped (LaO)CuS thin films showed around 60% transparency in the visible region with a room-temperature conductivity of $\sim 6.4 \times 10^{-5}$ S cm^{-1} (shown in Fig. 16). Films with Sr doping (3%) in the La sites show an increase in conductivity of almost six orders of magnitude to ~ 20 S cm^{-1} [119]. Divalent Sr^{+2} ions in the trivalent La^{+3} sites may act as acceptors increasing the hole concentration in the film as described by Eq. (2). On the other hand, heavy doping (20%) of Mg^{+2} ions in the La^{+3} sites of (LaO)CuSe films showed degenerate p-type conductivity with σ_{RT} ~ 140 S cm^{-1} (shown in Fig. 17). Also a systematic increase of the conductivity of (LaO)-CuS$_{1-x}$Se$_x$ ($x = 0$–1) films was observed with increasing Se content in the films (shown in Fig. 18). All the electrical and optical parameters are described in Table 2. It is worthwhile mentioning that all the similar types of layered oxychalcogenide materials of the form (LnO)MC^h (Ln = rare earth, La^{+3}, Pr^{+3}, Nd^{+3}, Sm^{+3}, Gd^{+3}, Y^{+3} etc.; M = Cu^{+1}, Ag^{+1}; C^h = S^{-2}, Se^{-2}) [122,127,129,131,136] may become promising materials for diverse applications in optoelectronics technology, but have yet to be explored completely. Tremendous opportunities lie ahead in this area of research.

4.4. Other mixed oxide films

Multicomponent oxide films of the form In$_2$O$_3$–Ag$_2$O have been reported by Minami et al. [137] to show p-type conductivity with low transmittance of $\sim 20\%$ in the visible region (shown in Fig. 19). In$_2$O$_3$ is a well-known n-type TCO with a bandgap (E_g) of 3.7 eV, whereas
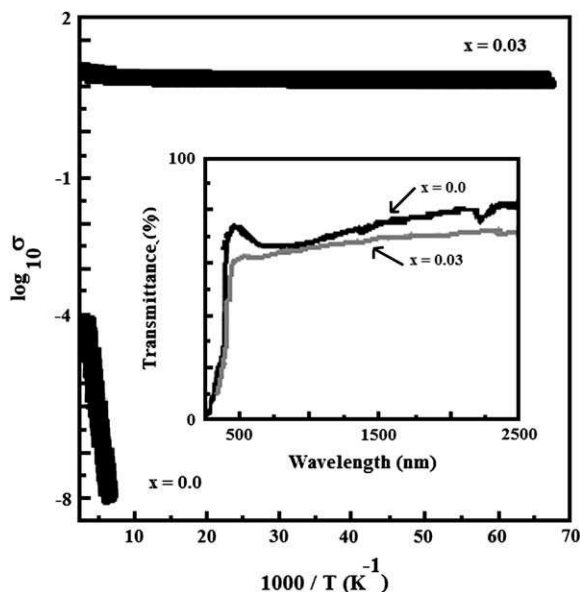
Fig. 16. Temperature variation of conductivity of undoped and Sr-doped (LaO)CuS thin films. Inset shows the optical spectra of undoped and Sr-doped (LaO)CuS thin films (after Ref. [119]).

Ag_2O is a p-type semiconductor with a smaller E_g of ~ 1.2 eV [138]. However, a mixture of these two materials with Ag_2O contents of 40 to 60 wt% showed p-type conduction. Post-deposition air annealing at an elevated substrate temperature (500 °C) of the film with 50 wt% Ag_2O content showed an increase in p-type conductivity upto a maximum value of
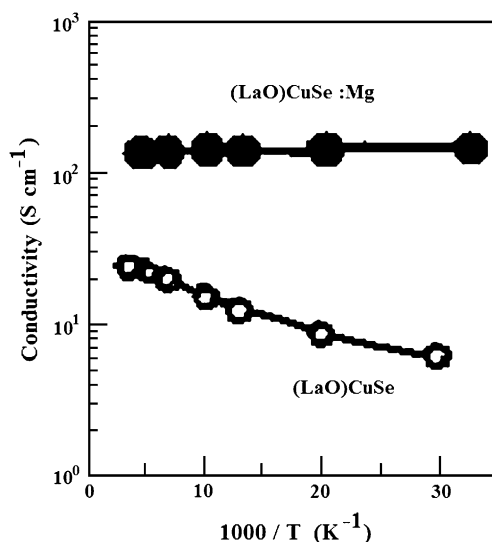

Fig. 17. Temperature dependence of undoped and Mg-doped (LaO)CuSe thin films (after Ref. [128]).
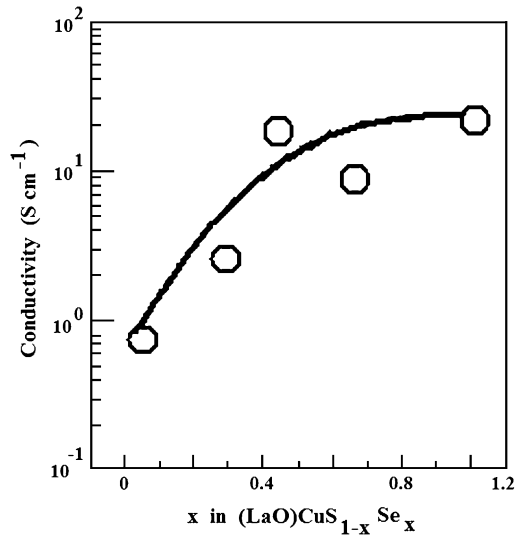
Fig. 18. Variation of room-temperature conductivity of $(LaO)CuS_{1-x}Se_x$ with change in x (after Ref. [128]).

$100 \, S \, cm^{-1}$ with an average of 20% visible transmittance. Excess oxygen within the film, induced due to air annealing may be the cause of the enhanced p-type conductivity of the films as described in Section 3.3, but exact stoichiometry has not yet been established.

4.5. Binary oxide films

Transparent binary metal oxides with p-type conductivity include NiO, doped ZnO (e.g. ZnO:N/As/P) etc. In fact NiO thin film was the first reported p-TCO [65] with a moderate 40% transparency in the visible region and a high $7.0 \, S \, cm^{-1}$ room-temperature conductivity.
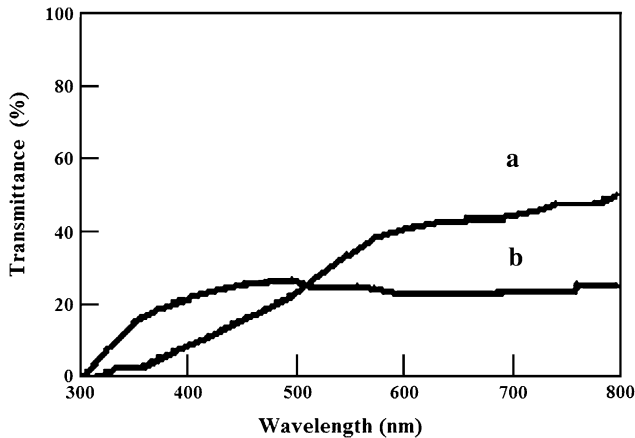

Fig. 19. Optical transmission spectra of (a) as-deposited, and (b) post-annealed (at 500 °C, for 1 h) $In_2O_3-Ag_2O$ thin film with 50 wt% Ag_2O content (after Ref. [137]).

The bandgap of NiO single crystal was reported to be between 3.6 and 4.0 eV [139,140]. Nickel oxide is a metal deficient material of the form $Ni_{1-x}O$ $(0 < x < 0.2)$ [141]. Antolini [142] proposed that both nickel vacancies as well as excess oxygen in interstitial sites are responsible for enhanced p-type conductivity of the material. Polycrystalline NiO has a rocksalt-type structure with cubic symmetry. Lattice parameters and band structure calculations were done in detail by various groups [141,143,144]. But there was a controversy on whether the carrier conduction in NiO is thermally activated conduction as often found in non-degenerate semiconductors or small polaron hopping type [140,141,145,146]. Hydrated NiO is also used as an active electrochromic material for various related applications [147−152]. Various optoelectrical parameters of NiO thin films are listed in Table 2.

p-Type ZnO thin film is another and a very important material in p-TCO technology. Doped versions of zinc oxides (ZnO:In/Al/F/B/Ga) are well-known and widely used transparent oxides with n-type conductivity [3,8,153]. The advent of p-ZnO is an important milestone in "Transparent Electronics" [64] due to the fact that p−n homo-junctions can be fabricated by both types of zinc oxide, which is a key structure in this field. The attempt to synthesize p-ZnO was first made long back in 1960 by Lander [154] and a decade later by Hümmer [155]. Later considerable efforts were made to produce p-ZnO doped with N [156−161] and As [162]. Recently, from a first principles calculation, Yamamoto and Yoshida [163] proposed that "co-doping" of donor−acceptor dopants (e.g. Ga and N, respectively) in ZnO might lead to p-type ZnO. Successful fabrication of p-ZnO by this theory has been achieved first by Joseph et al. [164]. In this method the simultaneous doping of both acceptor (N) and donor (Ga) into the ZnO lattice were carried out with an acceptor concentration twice that of the donor concentration to get a maximum conductivity in p-ZnO. The optical transmission spectrum of Ga co-doped p-ZnO thin film is shown in Fig. 20. The essential approach of this method is to stabilize the N substitution in the appropriate ZnO lattice sites by the formation of N−Ga−N type bonds, which reduce the N−N repulsive interaction (Madelung Energy) thereby making the acceptor level shallower, thus enhancing the acceptor doping [163,164]. But later on, several reports pointed out difficulties and a lack of reproducibility of p-ZnO using the "co-doping" technique [165−167a]. Although this raised some questions on "co-doping" theory, the failure to use proper growth parameters as well as formation of some non-ZnO species in the ZnO matrix in these studies may still be the cause of the ambiguous results. Recently, Triboulet and Perrière [167b] reviewed the advancement in the field ZnO films and briefly described the importance and recent status of p-ZnO films. This review dealt in detail with the various growth techniques for both n- and p-type epitaxial ZnO films and their device applications in optoelectronics, spintronics etc. This report and the corresponding references therein provide in-depth knowledge on the development of p-ZnO thin films. Tremendous scope lies ahead in this area of research for future applications.

4.6. Non-oxide p-type transparent semiconducting thin films

There are reports on the fabrication of non-oxide p-type transparent conductors like $BaCu_2S_2$, BaCuSF [168−170] etc. Park et al. [168] synthesized α-$BaCu_2S_2$ thin films, which crystallize at low temperature in an orthorhombic structure [171]. They obtained a visible transmittance of 70% for a 430 nm thick film with a rather low bandgap of 2.3 eV. The room-temperature conductivity was reported as 17 S cm^{-1} with a Hall mobility of 3.5 cm^{2}V^{-1} s^{-1}. Later the same group reported the preparation of undoped and K-doped BaCuSF pellets and thin films [170]. The transmittance of the undoped film was $\sim$85% in the visible region
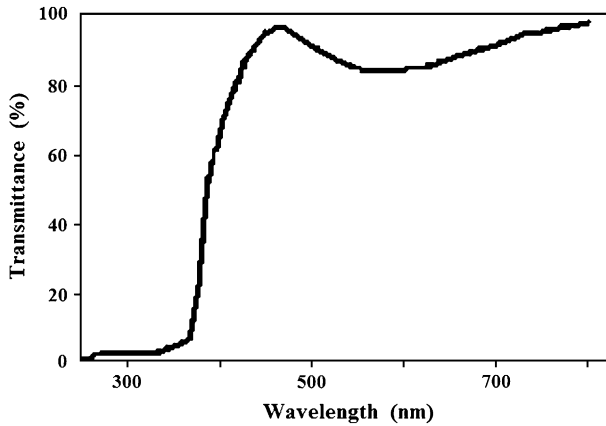
Fig. 20. Visible transmittance of p-ZnO thin film for 5 wt% Ga co-doped. N-doping was carried out using an N_2O flow (after Ref. [164]).

with an estimated direct bandgap value of 3.2 eV. A decrease in the transmittance with increase in the K-dopant was observed for the doped films. Room-temperature conductivity of the polycrystalline thin film was obtained as $1.0 \, S \, cm^{-1}$. Although these materials cannot be classified as p-TCO, they still have scientific importance in the field of ''Transparent Electronics''.

5. Deposition techniques

The actual technique for growth of thin films plays the most significant role in determining the properties of the films. Different deposition routes yield films with diverse structural, optical and electrical properties. Even for the same deposition technique, a slight variation in the deposition parameters produce films with different properties. So it is very important to have a comparative study on the properties of various films produced by different deposition routes. Detailed descriptions of different deposition techniques along with their schematic diagrams and related parameters are reported in various literatures [5,8,172—175]. In this section we have discussed the nature of the different growth techniques and corresponding deposition parameters of p-TCO thin films and tried to give a comparative study of the various techniques.

5.1. Pulsed laser deposition

Pulsed laser deposition (PLD) is a relatively new but very efficient technique to deposit epitaxial films. It is a somewhat costly process, but can produce high quality phase films with highly accurate thickness control. Films prepared by this method include $CuAlO_2$ [63,70,78,176], $CuGaO_2$ [70,87], $CuInO_2$:Ca [88], $CuScO_2$ [177], Cu_2SrO_2 [70,112], ZnO:N [164] etc. Relative comparison of PLD parameters for different thin films is furnished in Table 3. The deposition environment for most of the above-mentioned reports involved oxygen. In addition the films were grown at elevated substrate temperatures. Post-deposition annealing was also done in most cases to induce excess oxygen for enhancing p-type conductivity as described in Eq. (1). Temperature variation of conductivities, optical transmission spectra and X-ray diffraction (XRD) spectra of different pulsed laser deposited films are shown in Figs. 21—25.

Table 3
Deposition parameters for different p-TCO films grown by the PLD technique

	CuAlO$_2$	CuGaO$_2$	CuInO$_2$:Ca	CuScO$_2$	Cu$_2$SrO$_2$:K	ZnO:N
Laser	KrF (248 nm)	KrF (248 nm)	KrF (248 nm)	KrF	KrF (248 nm)	ArF
Laser frequency (Hz)	20	20	20	1	2	1
Laser power (J cm^{-2} pulse^{-1})	5	6	3.5	1.1	2.5	0.5
Base pressure (Pa)	1×10^{-7}	6×10^{-6}	1×10^{-7}	−	1×10^{-6}	1×10^{-6}
O$_2$ pressure (Pa)	1.3	9	1	1.5	7×10^{-4}	[a]
Target	CuAlO$_2$ pellet	CuGaO$_2$ pellet	CuInO$_2$:Ca pellet	Cu$_2$Sc$_2$O$_5$ pellet	Cu$_2$Sr$_{0.97}$K$_{0.03}$O$_2$ pellet	ZnO:Ga pellet
Substrate	α-Al$_2$O$_3$ (001)	α-Al$_2$O$_3$ (001)	α-Al$_2$O$_3$ (001)	α-Al$_2$O$_3$ (1120)	SiO$_2$	SiO$_2$
Substrate−target distance (mm)	25	25	25	40	40	−
Substrate temperature (°C)	690	700	450	900	300	400
Deposition time (min)	−	−	−	−	180	−
Post-annealing time (min)	180	None	None	None	120	−
Post-annealing temperature (°C)	690	None	None	None	300	−
Reference	70,78	70,87	88	177	70,112	164

[a] The deposition atmosphere was N$_2$ or N$_2$O.

5.2. Sputtering

Sputtering is one of the most popular thin film growth techniques around the globe. As it is relatively cost-effective compared with PLD and large-area deposition is possible by this process, large-scale production of films for diverse applications can be carried out by this
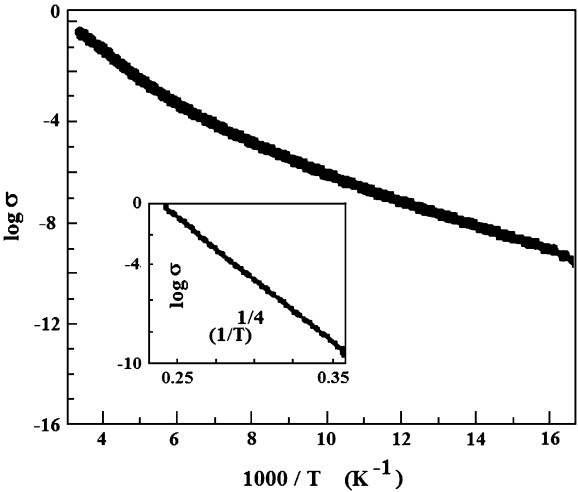

Fig. 21. Temperature variation of conductivities of pulsed laser deposited CuAlO$_2$ thin films from room temperature (∼30 °C) to −53 °C. Inset shows the same below −53 °C, indicating two different conduction regimes. Above −53 °C the conduction mechanism is thermal activation type whereas below −53 °C a variable-range hopping mechanism becomes dominant (after Ref. [78]).
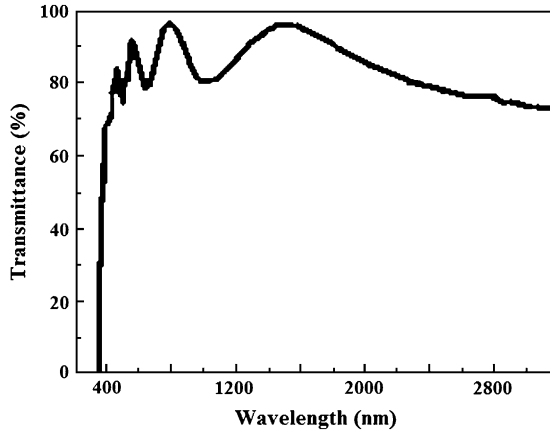
Fig. 22. Optical transmission spectra of a CuGaO$_2$ thin film deposited by the PLD technique (after Ref. [87]).

technique. Both reactive and non-reactive forms of direct current (d.c.), radio frequency (r.f.), magnetron as well as ion beam sputtering techniques have been used for the deposition of various p-TCOs.

r.f. magnetron sputtering of CuAlO$_2$ [176], CuGa$_{0.5}$Fe$_{0.5}$O$_2$ [66], CuCr$_{0.95}$Mg$_{0.05}$O$_2$ [95], CuScO$_{2+y}$, CuSc$_{0.95}$Mg$_{0.05}$O$_2$ [94,66], CuNi$_{0.67}$Sb$_{0.3}$Sn$_{0.033}$O$_2$ [66,68], AgCoO$_2$ [66], NiCo$_2$O$_4$ [117], (LaO)CuS [123], (La$_{1−x}$Sr$_x$O)CuS [118,119,126], NiO [65], In$_2$O$_3$−Ag$_2$O [137], and Cu$_2$BaS$_2$ [168] have been reported. On the other hand d.c. sputtering of CuAlO$_2$ thin film has been reported [178−181] by us, which is a more cost-effective procedure. Also, in d.c.
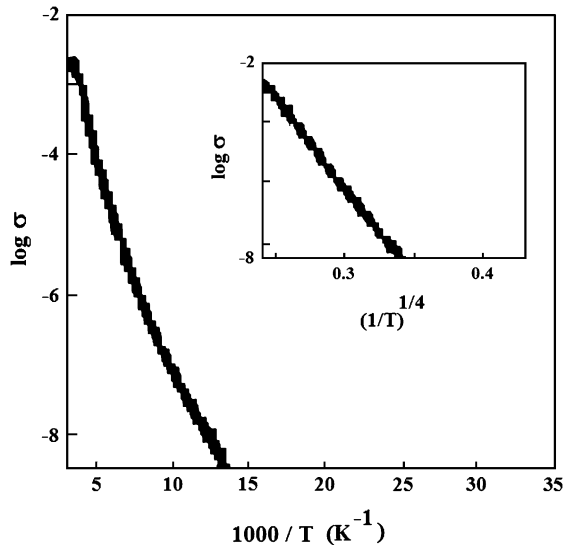

Fig. 23. Temperature variation of conductivity of CuInO$_2$:Ca thin film deposited by PLD method, indicating two different conduction mechanisms. Above −73 °C thermally activated conduction and below −73 °C variable-range hopping type conduction are taking place (after Ref. [88]).
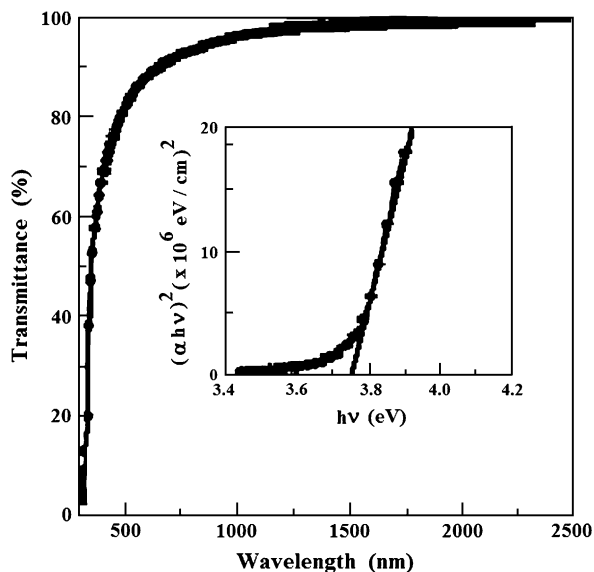
Fig. 24. Optical transmission spectra of $CuScO_2$ thin film. Inset shows the determination of the direct bandgap (after Ref. [177]).

sputtering of oxide targets, the control of stoichiometry is almost automatic, whereas for r.f. sputtering, the target stoichiometry has to be adjusted suitably to compensate material loss from the substrate [8]. In all of the above-mentioned reports, the targets used were the corresponding sintered pellets, arranged properly in the deposition chamber.

r.f. magnetron reactive co-sputtering of Cu and Al metal targets was used by Ong and Gong [182] to synthesize transparent p-type Cu−Al−O films (a mixture of $CuAlO_2$ and CuO). It is well known that for low resistive targets, d.c. sputtering can be applied conveniently whereas r.f. sputtering can also be applied for highly resistive (or insulating) targets. So keeping an eye on the cost-effectiveness of the deposition techniques, d.c. reactive sputtering of films
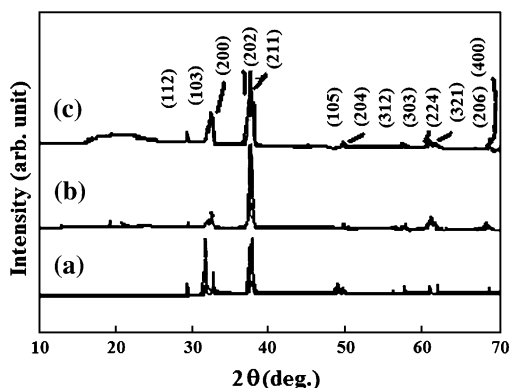

Fig. 25. XRD patterns of (a) Cu_2SrO_2 pellet, (b) K-doped Cu_2SrO_2 thin film, and (c) undoped Cu_2SrO_2 thin film deposited by PLD technique (after Ref. [112]).

from metal targets has been adopted by various groups. Tsuboi et al. [183] used opposite facing targets of Cu and Al metals and a rotating substrate to synthesize $CuAlO_2$ films by d.c. reactive sputtering (a schematic diagram of the apparatus is shown in Fig. 26). In our previous work, we have prepared $CuAlO_2$ thin films by d.c. reactive sputtering of a mixture of Cu and Al metal powder pellets [184]. Reactive sputtering has the advantage over conventional (r.f. or d.c.) sputtering from oxide targets, due to the fact that the plasma density would be better in the former case due to the high conductivity of elemental targets or metal powders, leading to better uniformity of the films. Also the intermediate step of a sintering procedure to form the target pellet can be avoided by this method. It must be mentioned here that in most of the sputtering procedures indicated above, the sputtering atmospheres were taken as Ar and O_2 and the depositions were done at an elevated substrate temperature. Post-annealing of the films was also performed in many cases to get better p-type conductivity. In some cases, rapid thermal annealing (RTA) of the films was also carried out to get higher crystallinity and transparency [94,95]. Different deposition parameters of various sputter-deposited p-TCO thin films are furnished in Table 4. Also XRD patterns, optical spectra and temperature variation of conductivities and Seebeck coefficients of various sputter-deposited thin films are shown in Figs. 27—36.

5.3. Chemical vapor deposition

Chemical vapor deposition (CVD) is another widely used growth technique. The importance of this method lies in the fact that the vapors of liquid materials can be used here in a controlled manner. Also a wide variety of reactant species ranging from inorganic compounds to organo-metallic liquids can be used in this process. Although high purity films can be produced by this technique, the morphology of the films is highly correlated with the nature of the chemical reactions and activation mechanisms during the process. The reaction must not occur far away from the surface of the substrate so that powdery deposits are formed on the substrate leading to hazy films, which is undesirable for TCOs [8].
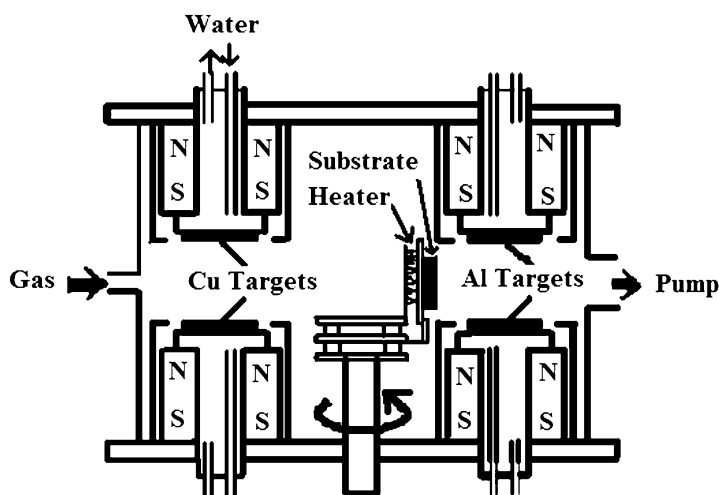

Fig. 26. Schematic representation of d.c. reactive sputtering system with two pairs of opposite facing targets and a rotating substrate (after Ref. [180]).

Depositions of p-type transparent Cu−Al−O (a mixture of $CuAlO_2$ and Cu_2O) films by plasma-enhanced metal-organic CVD (PE-MOCVD) were performed by Gong and co-authors [185−187]. They have used metal-organic powder precursors of $Cu(dpm)_2$ and $Al(dpm)_2$ (dpm → dipivaloylmethanate) with a 1:1 molar ratio and evaporated the mixture at 150 °C. The carrier gas was Ar (30 sccm) whereas the reactive gas was O_2 (30 sccm). The substrate temperature and working pressure were 830 °C and 20 Pa [185], respectively. This group, in a similar way, deposited Cu−Al−O films by PE-MOCVD technique using $Cu(acac)_2$ and $Al(acac)_2$ precursors (acac → acetylacetonate) on a quartz substrate at a substrate temperature of 745 °C. The Ar and O_2 flow rates were 25 and 18 sccm, respectively, whereas the working pressure was 6.67 Pa [186]. In both cases the base pressures were kept at 4×10^{-4} Pa. Various electrical and optical properties of chemical vapor deposited Cu−Al−O thin films are shown in Figs. 37 and 38.

Amongst binary oxides, NH_3-doped ZnO (basically ZnO:N) with p-type conductivity was reported by Wang et al. [159]. They have used diethyl zinc (DEZn), O_2 gas and NH_3 as zinc, oxygen and nitrogen sources, respectively, whereas the carrier gases were a mixture of Ar and N_2. They observed that the films deposited with 50 sccm NH_3 flux during deposition showed the best p-type nature. The substrate was sapphire (0 2 $\bar{2}$ 4) and the deposition time was 10 min [159].

5.4. Other physical techniques

5.4.1. Reactive solid-phase epitaxy

Reactive solid-phase epitaxy (R-SPE) technique [188,189] was employed to deposit (LaO)CuS and $(LaO)CuS_{1-x}Se_x$ films on MgO (001) and yittria-stabilized-zirconia (YSZ) substrates [127,128,190]. It is essentially a two-step growth technique. First, a fine layer of metallic copper (∼5 nm) was deposited on the substrate by the PLD method under a high vacuum (∼10^{-5} Pa) and at an elevated substrate temperature (400 °C). Thereafter layers of (LaO)CuS and (or) (LaO)CuSe were sequentially deposited on the Cu-deposited substrate (at 25 °C) from the corresponding sintered pellets by the PLD technique. Finally, the multilayer film was post-annealed at 1000 °C to get the required epitaxial thin film. The copper layer was supposed to act as an "epitaxy initiator" [190].

5.4.2. Molecular beam epitaxy

Transparent p-type conducting nitrogen doped zinc oxide (ZnO:N) films were grown by the molecular beam epitaxy (MBE) technique on ZnO substrates [160]. Nitrogen doping was carried out by incorporation of an N_2 flux into the MBE system along with an O_2 flow with an N_2 level 10 to 100 times less than the O_2 gas level. In a similar way, H_2O vapor assisted metalorganic molecular beam epitaxy (MO-MBE) technique was used by Ashrafi et al. [161] to obtain p-type ZnO:N thin films. Zinc and nitrogen sources were taken as diethyl zinc (DEZn) and monomethyl hydrazine (MMHy), respectively, and the substrate used was sapphire, which was kept at a temperature of 400 °C during deposition and subsequently annealed in an O_2 ambient at 700 °C for 20 min.

5.4.3. Thermal co-evaporation

Reactive thermal co-evaporation of Cu, Y and Ca metal powders in a reactive O_2 atmosphere (0.02 Pa) to form $CuY_{1-x}Ca_xO_2$ thin films on glass, MgO (100) and Si substrates were reported by Jayaraj et al. [96]. Deposition was carried out at an elevated substrate temperature (80−650 °C). RTA of the films was also performed (for 1 min at 400 °C) to get better

Table 4

Different deposition parameters of p-TCO films synthesized by the sputtering method

(A) r.f. magnetron sputtering

Material	CuAlO$_2$	CuGaO$_2$:Fe	CuCrO$_2$:Mg	CuNi$_{2/3}$Sb$_{1/3}$O$_2$:Sn	AgCoO$_2$	NiCo$_2$O$_4$	(LaO)CuS	NiO	In$_2$O$_3$−Ag$_2$O
r.f. power (W)	65	80	90	80	80	200	110	50	40
Electrode distance (mm)	40	30	38	−	30	−	35	−	−
Base pressure (Pa)	−	−	9.3×10^{-4}	−	−	1.33×10^{-4}	−	−	−
Sputtering pressure (Pa)	4.53 (O$_2$ press)	13.33 (Ar:O$_2$ = 4:1)	1.33 (Ar press)	13.33 (Ar:O$_2$ = 4:1/9:1)	53.33 (Ar:O$_2$ = 4:1)	1.33	13 (Ar:H$_2$S = 19:1)	0.8 (O$_2$ press)	0.25 (Ar + O$_2$)
Target	CuAlO$_2$ pellet	CuGa$_{0.5}$Fe$_{0.5}$O$_2$ pellet	CuCr$_{1−x}$MgO$_2$ pellet	CuNi$_{0.67}$Sb$_{0.3}$−Sn$_{0.03}$O$_2$ pellet	AgCoO$_2$ pellet	Co−Ni alloys	(LaO)CuS:Sr pellet	NiO pellet	In$_2$O$_3$−Ag$_2$O pellet
Substrate	α-Al$_2$O$_3$ (001)	Fused silica	Fused quartz	SiO$_2$, YSZ (100), Al$_2$O$_3$ (001)	SiO$_2$, Al$_2$O$_3$	Quartz, sapphire, Si	SiO$_2$	SiO$_2$	SiO$_2$
Substrate temperature (°C)	Ambient	100 °C	450−750	500 °C	400 °C	Ambient	Ambient	200	Ambient
Post-annealing time (min)	90	90	2.5 (RTA in Ar)	180	−	−	120	None	60
Post-annealing temperature (°C)	1050[a]	800 °C (N$_2$ atmos.)	600−900	900 °C (in air)[c]	−	−	800[b]	None	500
Reference	176	66	95	66,68	66	117	119	65	137

(B) r.f. magnetron reactive sputtering

Material	Cu−Al−O films (a mixture of CuAlO$_2$ and Cu$_2$O)	p-ZnO
r.f. power (W)	Al power, 60−110[d]; Cu power, 30 W	20
Targets	Metallic Cu and Al	Metallic Zn
Substrate	Glass	Si (100)
Substrate temperature (°C)	100	350
Sputtering atmosphere	Ar + 5% O$_2$	Ar + 83% O$_2$ (pressure ∼4 Pa)
Post-annealing	None	At 750 °C, in vacuum ($\sim 1.33 \times 10^{-4}$ Pa), for 30 min.
Reference	179	199

(C) d.c. sputtering

Material	CuAlO$_2$ thin film
Electrode distance (mm)	18

Target		Sintered $CuAlO_2$ pellet
Substrate		Si (400) and glass
Sputtering voltage (V)		1100
Current density (mA cm^{-2})		10
Base pressure (Pa)		10^{-4}
Sputtering pressure (Pa)		20
Sputtering atmosphere		Ar + 40 vol% O_2
Substrate temperature (°C)		180
Deposition time (min)		240
Post-annealing time (min)		60
Post-annealing temperature (°C)		200
Post-annealing atmosphere (pressure)		O_2 (20 Pa)
Reference		178

(D) Reactive d.c. sputtering

Material	$CuAlO_2$ thin film	$CuAlO_2$ thin film
Target	Elemental Cu and Al metal (facing) targets	Mixture of Cu + Al metal powder pellets
Electrode distance (mm)	−	18
Sputtering voltage (V)	Cu facing targets = 750 V, Al facing targets = 350 V	1000
Current density (mA cm^{-2})	Cu facing targets ∼1.17, Al facing targets ∼7.0	12
Base pressure (Pa)	−	10^{-4}
Sputtering pressure (Pa)	0.53	20
Sputtering atmosphere	Ar + O_2 (4:1)	Ar + O_2 (3:2)
Substrate	Quartz (rotating)	Si (400) and glass
Substrate temperature (°C)	300	200
Deposition time (min)	240	240
Post-annealing time (min)	240	120
Post-annealing temperature (°C)	>700	220
Post-annealing atmosphere	N_2 (ambient pressure)	O_2 (20 Pa)
Reference	180	181

[a] Ex situ in a Lindberg box furnace containing small amount of $CuAlO_2$ powder.
[b] Ex situ in an evacuated silica tube containing small amount of (LaO)CuS powder.
[c] Also for some cases RTA in air at 900 °C was performed.
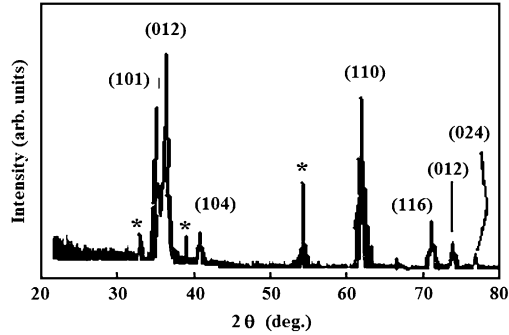[d] For Al power 110 W single-phase amorphous $CuAlO_2$ was formed.

Fig. 27. XRD pattern of $CuCr_{0.95}Mg_{0.05}O_2$ thin film deposited by the r.f. sputtering technique (after Ref. [95]). "*" marks are from the indium contacts.

crystallinity and conductivity of the films. The film showed an average of 50% transparency (shown in Fig. 39) in the visible region. Synthesis of phase-pure $CuGaO_2$ thin film on fused silica by the thermal co-evaporation technique from elemental Cu and Ga in an O_2 atmosphere was also reported by this group [66]. Similarly, non-oxide p-type conducting transparent films of BaCuSF were also deposited by the co-evaporation technique from metals Cu and BaF_2 on SiO_2 and MgO substrates held at 200 °C and subsequently post-annealed at 350 °C for 3 h under an H_2S atmosphere [111]. The deposition parameters of different co-evaporation methods used for growth of various p-TCO thin films are described in Table 5.

5.4.4. Electron-beam evaporation

Electron-beam (e-beam) evaporation of $SrCu_2O_2$ pellets was performed to deposit p-type transparent Sr—Cu mixed oxide thin films on glass and quartz substrates in an oxygen atmosphere (0.067 Pa) [191]. The substrate temperature was varied from 250 °C to 350 °C whereas post-annealing was performed in both O_2 and N_2 atmospheres as well as in vacuum at an elevated substrate temperature of 350 °C. Optical transmittance and reflectance spectra of Sr—Cu mixed oxide thin films deposited at a substrate temperature of 250 °C and 0.05 Pa O_2 pressure are shown in Fig. 40. The films showed around 60% transparency in the visible region.
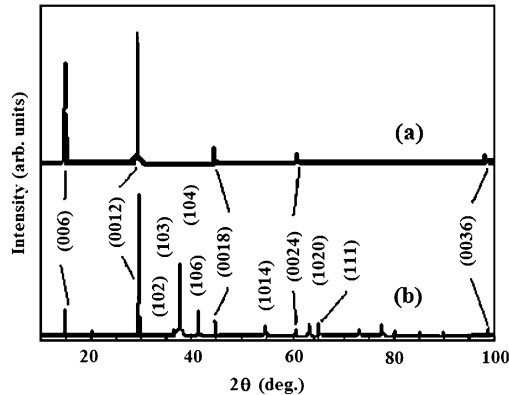

Fig. 28. XRD pattern of (a) $AgCoO_2$ thin film deposited by r.f. sputtering, and (b) target (after Ref. [66]).
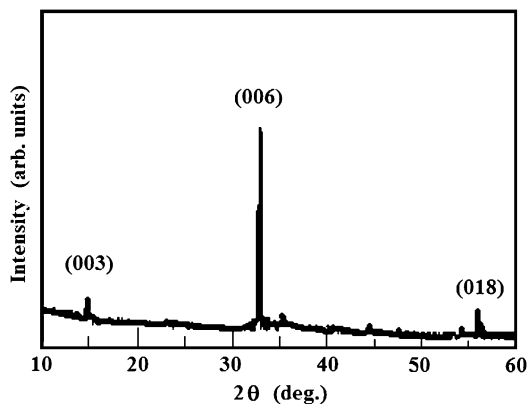
Fig. 29. XRD pattern of d.c. sputtered deposited $CuAlO_2$ thin film (after Ref. [178]).

5.4.5. Other methods

Ion exchange method is another interesting procedure by which several delafossite materials have been synthesized such as $CuAlO_2$ from $LiAlO_2$ [192], $CuInO_2$ from CuCl, Ag_xCoO_2 ($x < 1$) from $NaCoO_2$ and $AgNO_3$ [66], $AgNi_{0.67}Sb_{0.33}O_2$ from $LiNi_{0.67}Sb_{0.33}O_2$ and $AgNO_3$ [68], $AgZn_{0.67}Sb_{0.33}O_2$ from $LiZn_{0.67}Sb_{0.33}O_2$ and $AgNO_3$ [68] etc. Although no film preparation was reported by this method this process may become an important target preparation procedure for PLD or sputtering.

Also, based on ab initio electronic structure calculations, new methods have been proposed by Yoshida and co-authors [193,194] to fabricate highly conducting p-$CuAlO_2$. They proposed that in thermal non-equilibrium PLD or molecular beam epitaxy (MBE) crystal growth techniques, the introduction of a high concentration of Cu vacancies occurs in the material, to form an impurity band. Reducing the Cu vapor pressure during deposition might enhance the p-type conductivity in the material. On the other hand, doping of Mg or Be at Al sites to form acceptor levels by decreasing the Al vapor pressure and increasing the Cu vapor pressure during low-temperature PLD, MBE or MOCVD process might also increase the p-type conductivity of the material.
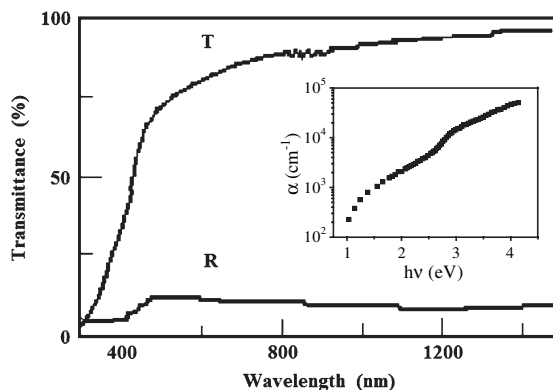

Fig. 30. Optical transmittance and reflectance spectra of $CuAlO_2$ thin film deposited by d.c. sputtering. Inset shows the spectral variation of absorption coefficients (α) (after Ref. [178]).
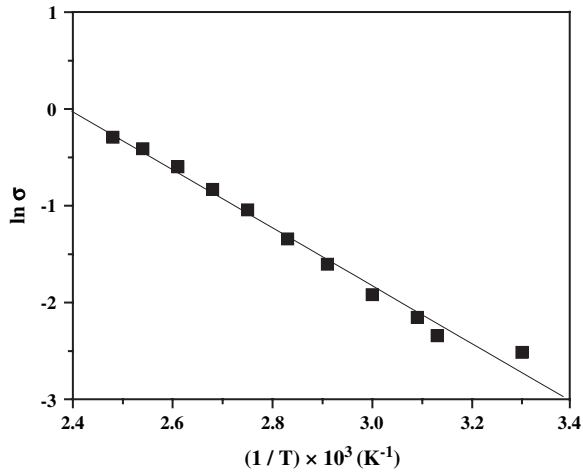
Fig. 31. Temperature variation of conductivity of CuAlO$_2$ thin film deposited by d.c. sputtering (after Ref. [178]).

5.5. Wet-chemical synthesis

Wet-chemical solution-growth technique is another popular method for its simplicity and cost-effectiveness. Various authors have tried to grow p-TCO films by this process. The first report of porous copper−aluminum−oxide was published more than a decade ago by Patrick and Gavalas [195], where the citrate process [196] was adopted. But as porous material is not favorable for high conductivity applications, sol−gel and nitrate routes were adopted later by Tonooka et al. [197] to deposit Cu−Al−O films (a mixture of CuAlO$_2$, CuAl$_2$O$_4$ and CuO) for possible high performance applications in p-TCO technology. Three precursor solutions were prepared (two for the sol−gel-dip-coating process and one for the nitrate process) and the films were deposited on Si substrates. Films produced by the nitrate route showed a higher percentage of CuAlO$_2$ phase in the film than the sol−gel routes. On the other hand Shahriari et al. [109] synthesized CuAlO$_2$ and Ga doped CuAlO$_2$ solid solutions by a hydrothermal
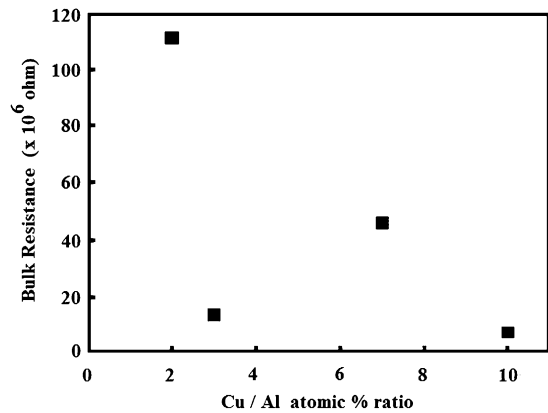

Fig. 32. Bulk resistance of Cu−Al−O thin films with different Cu/Al atomic ratios (after Ref. [179]).
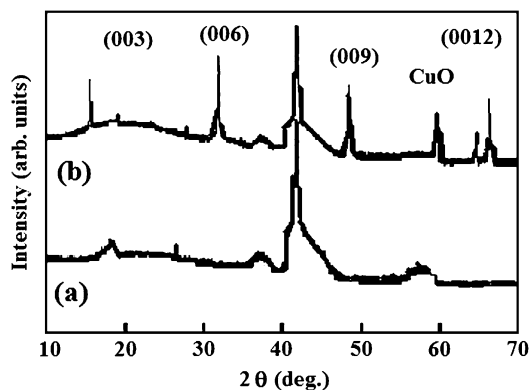
Fig. 33. XRD patterns of $CuAlO_2$ thin films deposited by r.f. magnetron sputtering (a) as-deposited film, (b) post-annealed at 1050 °C (after Ref. [176]).

process. Although thin film preparation was not reported by this method it is an important step towards the thin film growth of p-TCOs by the chemical route. Similarly, Tate et al. [66] prepared Ag-based delafossite p-type conducting $AgCoO_2$ powder by a four-day hydrothermal reaction in a Parr bomb at 250 °C, which was used as a sputtering target to synthesize the corresponding film. Recently we have synthesized highly oriented $CuAlO_2$ thin films from copper and aluminum chloride solution by a wet-chemical dip-coating route [198]. The films showed high transparency but a low p-type conductivity. The optical transmission spectra of these films are shown in Fig. 41 whereas the direct bandgap calculations are shown in Fig. 42.

The solution-growth technique adopted for other p-TCOs includes transparent Co–Ni–O spinel films [115]. Spin-coating from a precursor solution of nickel and cobalt nitrates were used to deposit Ni–Co–O (a mixture of $NiCo_2O_4$, NiO and Co_3O_4) thin films.

Flow-charts for different solution-growth techniques are shown in Fig. 43. Also the electrical and optical properties of various p-TCO thin films deposited by different processes are compared in Tables 6–8.
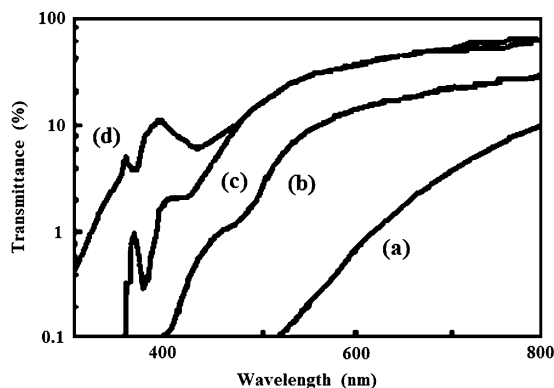

Fig. 34. Optical transmission spectra of Cu–Al–O films post-annealed at 1050 °C. Cu/Al ratio of the films are (a) 1.8, (b) 1.7, (c) 1.1 and (d) 0.7 (after Ref. [180]).
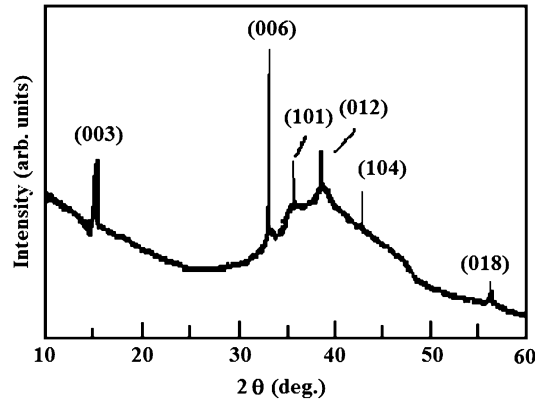
Fig. 35. XRD pattern of CuAlO$_2$ thin film deposited by reactive d.c. sputtering (after Ref. [181]).

6. All-TCO junctions

Junction devices fabricated by both n and p-type TCO thin films are the key structure for ''In-visible Electronics'' [64]. The simplest of them is the p–n junction diode with rectifying prop-erties. The importance of these types of devices lies in the fact that ''functional windows'' can be fabricated by these devices, which allow the transmission of visible solar radiation but absorb the UV [63]. Thus simultaneously these devices can act as ''UV-shields'' as well as ''electricity gen-erators'' by the UV absorption. Fabrications of a number of all-TCO diodes have been reported, which include both p–n and p–i–n homo-junctions and hetero-junctions.

The first all-TCO diodes were reported by Sato et al. [65]. They fabricated a semi-transpar-ent thin film of p–i–n structure consisting of p-NiO/i-NiO/i-ZnO/n-ZnO:Al. The thicknesses of the p-layer and n-layer were 195 and 400 nm, respectively. The rectifying properties of the structure confirmed the formation of the junction. They also tried to fabricate p–n diodes of the form p-NiO/n-ZnO:Al. But they observed linear I–V characteristics in both forward and
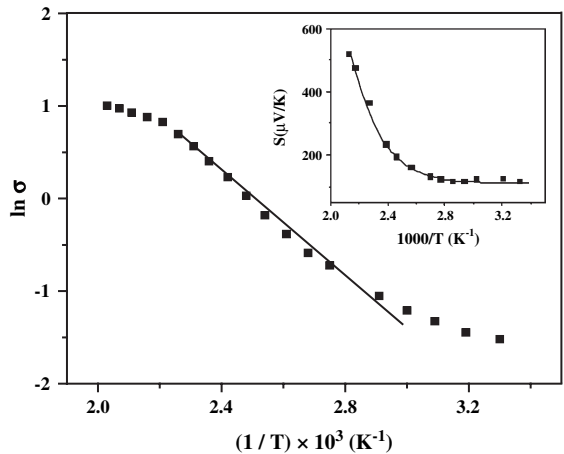

Fig. 36. Temperature variation of conductivity of reactive d.c. sputtered CuAlO$_2$ thin film. Inset shows the temperature dependence of the Seebeck coefficients (S) of the same (after Ref. [181]).
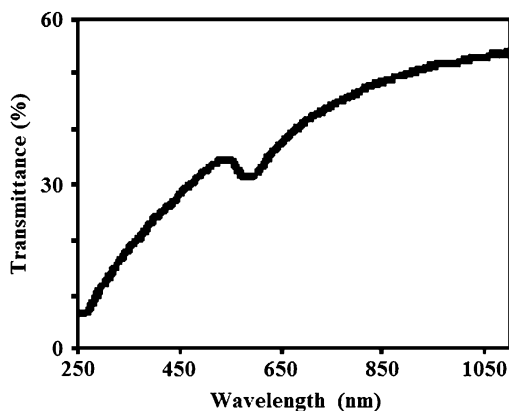
Fig. 37. Optical transmittance spectra of Cu−Al−O thin films deposited by CVD technique (after Ref. [183]).

reverse directions. Similarly, fabrication of all-TCO p−n hetero-junction thin film diode of the form p-SrCu$_2$O$_2$/n-ZnO was reported by Kudo et al. [199]. A schematic diagram of the diode structure is shown in Fig. 44(a) and the corresponding I−V characteristics in Fig. 44(b). The same group also reported UV emission from a p−n hetero-junction diode composed of p-SrCu$_2$O$_2$/n-ZnO after current injection through it [200−203]. p−i−n hetero-junction in the form of p-SrCu$_2$O$_2$:K/i-ZnO/n-ZnO was also constructed by this group [202]. Similarly a p−i−n hetero-junction of the form p-CuYO$_2$:Ca/i-ZnO/n-ITO was fabricated by Hoffman et al. [204]. The diode structure and I−V characteristics are shown in Fig. 45(a) and (b). Lattice matching is one of the most important requirements for realizing rectifying junctions. In most of the reports on the p−n hetero-junctions published so far, n-ZnO and p-SrCu$_2$O$_2$ were used as the n and p-layers, respectively, because of lattice matching between them. Also the low deposition temperature ($\sim$350 °C) of SrCu$_2$O$_2$ made it possible to minimize the chemical reaction at the SrCu$_2$O$_2$−ZnO interface.
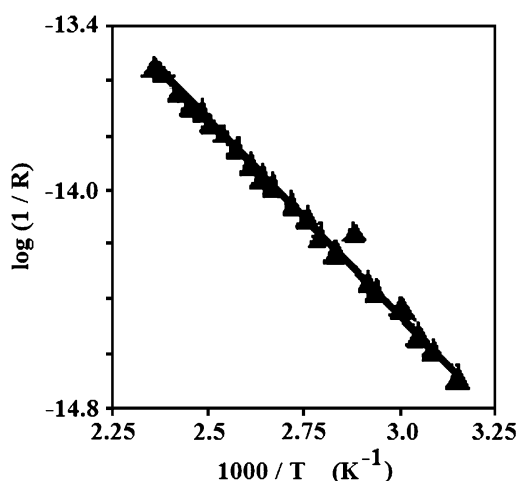

Fig. 38. Temperature variation of electrical conduction of Cu−Al−O thin film deposited by the CVD method (after Ref. [183]).
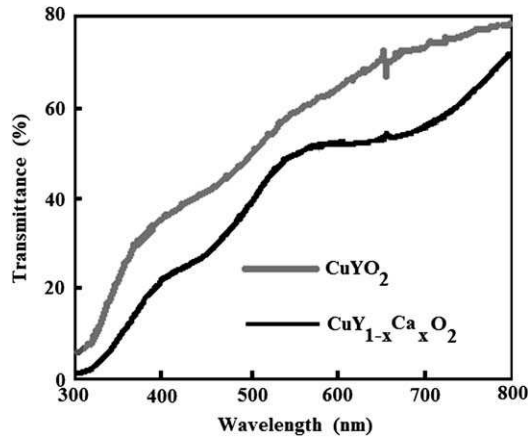
Fig. 39. Optical transmittance spectra of undoped and Ca-doped $CuYO_2$ thin films deposited by the thermal co-evaporation technique (after Ref. [96]).

Lastly, carrier concentration in ZnO can be controlled easily by varying the O_2 partial pressure during deposition in order to match the hole concentration in $SrCu_2O_2$ [199,201,202]. Jayaraj et al. [96,205] fabricated p−n hetero-junction using $p-CuY_{1−x}Ca_xO_2$ ($x = 0.01−0.02$)/$n-Zn_{1−x}Al_xO$ ($x = 0.02$) structure. They observed rectifying $I−V$ characteristics with a turn-on voltage between 0.4 and 0.8 V (shown in Fig. 46). Tonooka et al. [206] reported the fabrication of $n-ZnO/p-CuAlO_2$ diode structure with rectifying characteristics and observed a photovoltaic effect (as large as 80 mV) under illumination with blue radiation. Although the performance of the diode was restricted by the low crystallinity of the $CuAlO_2$ layer the forward-to-reverse current ratio showed a moderate value of 90 between −1.5 and +1.5 V. Also the transparency of the structure was 40% to 70% in the visible region. The transparency of the diode is shown in Fig. 47.

Besides hetero-junctions, fabrication of p−n homo-junctions was also reported by a few authors. The importance of the homo-junctions lies in the fact that lattice matching is supposed to be automatic during the formation of diodes. First all-delafossite p−n homo-junction diode was fabricated by Yanagi et al. [89]. The diode structure was of the form of YSZ (111)/ITO/$p-CuInO_2:Ca$/$n-CuInO_2:Sn$/ITO (shown in Fig. 48(a)). Calcium and tin-doped copper indium

Table 5
Deposition parameters for various co-evaporation techniques

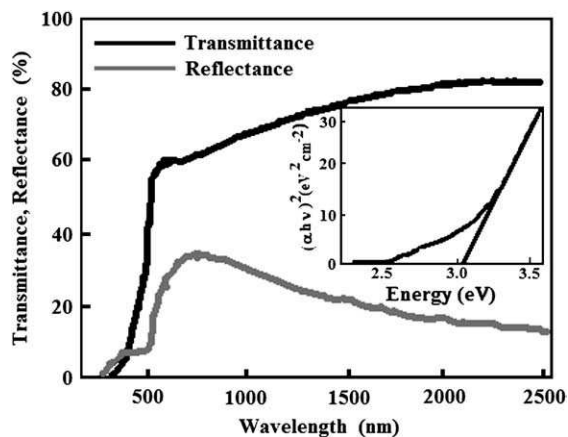| Material	$CuYO_2:Ca$[a]	$CuGaO_2$	BaCuSF
Reactants	Elemental Cu, Y, Ca metals	Cu, Ga metals	Cu metal, BaF_2
Base pressure (Pa)	9.33×10^{-5}	9.33×10^{-5}	−
Reactant gas	O_2	O_2	H_2S
Deposition pressure (Pa)	0.02	0.02	−
Substrate	Glass, MgO (100), Si	SiO_2	SiO_2, MgO
Substrate temperature (°C)	80−650	100	200
Post-annealing time (min)	3 (RTA)	90	180
Post-annealing temperature (°C)	600	800	350
Post-annealing atmosphere	O_2	N_2	H_2S
Reference	96	66	111

[a] 1−2% Ca doping in Y sites.

Fig. 40. Optical transmittance and reflectance spectra of copper−strontium mixed oxide thin films deposited by e-beam evaporation. Inset shows the calculation of direct bandgap (after Ref. [188]).

oxide films were used as the p and n-layers whereas ITO was used for the metallic electrodes. They observed rectifying properties of the junction with a turn-on voltage of ~ 1.8 V, which is shown in Fig. 48(b). Similarly all-ZnO p−n homo-junctions were reported by Hwang et al. [207], Tüzemen et al. [208] and Aoki et al. [209]. Hwang et al. [207] fabricated n-ZnO:Al/p-ZnO:As and observed rectifying characteristics with a turn-on voltage around 2.5 V (shown in Fig. 49). Tüzemen et al. [208] reported intrinsic p and n-type ZnO homo-junctions, prepared by reactive r.f. magnetron sputtering. The n-type and p-type conductivities were obtained by varying O_2 partial pressure in the $Ar + O_2$ sputtering atmosphere. A total of 4 Pa atmosphere pressure of Ar with 50% O_2 produced n-ZnO whereas Ar with 83% O_2 again at a total 4 Pa pressure produced p-ZnO. The diode characteristics are shown in Fig. 50. It is worthwhile to note that the first report of p-type conductivity in intrinsic ZnO was reported by Butkhuzi et al. [210], where post-annealing of the as-grown material in an atomic oxygen atmosphere was performed to achieve intrinsic p-type conductivity. Aoki et al. [209] fabricated p-ZnO:P/n-ZnO homo-junction and observed rectifying $I−V$ characteristics. Phosphorous
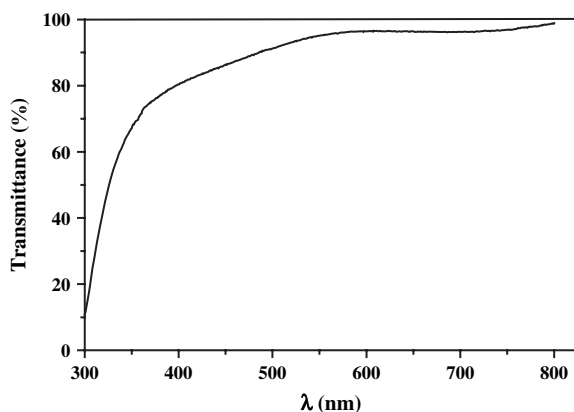

Fig. 41. Optical transmission spectra of a dip-coated copper aluminum oxide thin film.
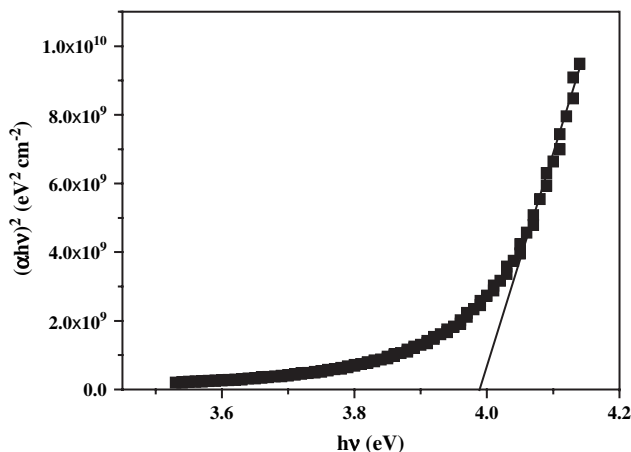
Fig. 42. Determination of the direct bandgap (after Ref. [195]).

doping was performed using an excimer-laser doping procedure with Zn_3P_2 as the phosphorous source. If the carrier concentration could be increased by optimizing the deposition parameters then these all-ZnO diode structures may open up a new horizon in the field of "Transparent Electronics". Various parameters of different all-transparent diodes are shown in Table 9.

Another important area in the field of "Transparent Electronics" is the fabrication of transparent field-effect transistors (TFET) [211]. Prins et al. [212,213] reported the fabrication of ferroelectric TFETs, based on transparent SnO_2:Sb thin films. They have observed a field-effect mobility of around $10\,cm^2\,V^{-1}\,s^{-1}$, with an on/off current ratio of $\sim 10^4$. Later various groups [214–216] reported the fabrication of ZnO based TFETs with reasonable device properties. Hoffman et al. [214] reported 75% visible transparency in their ZnO-TFETs with mobility and on/off ratio around $2.5\,cm^2\,V^{-1}\,s^{-1}$ and 10^7, respectively. Masuda et al. [215] observed these values around $1.0\,cm^2\,V^{-1}\,s^{-1}$ and 10^5, respectively, with an optical transmittance of more than 80% in the visible region. Similarly Carcia et al. [216] obtained these values around $2.0\,cm^2\,V^{-1}\,s^{-1}$, 10^6 and $>80\%$, respectively, for their ZnO-TFETs. Recently, Nomura, Ohta and co-authors [217,218] reported the successful fabrication of high mobility top-gate TFETs based on single-crystalline transparent $InGaO_3(ZnO)_5$ thin film. The device shows the mobility as high as $80\,cm^2\,V^{-1}\,s^{-1}$ with an on/off current ratio of $\sim 10^6$ and more than 80% transparency in the visible and near infrared region. The deposition techniques for the fabrication of these TFETs include pulsed laser deposition (PLD) [212,213,215], ion beam sputtering [214], r.f. magnetron sputtering [216], reactive solid-phase epitaxy [217] etc. The deposition routes and various parameters of different TFETs are shown in Table 10. These reports provide a significant step towards the achievement of "Invisible Electronics".

7. Nanocrystalline p-TCO thin films for nanoactive devices

After the pioneering works of Efros and Efros [219] and Brus [220] on the size-quantization effect in semiconductor nanoparticles, the research on nanostructured materials generates a great interest in the scientific community and offers tremendous opportunities in the field of physics, chemistry, materials science and related interdisciplinary areas because of new properties

Fig. 43. Flow-charts of different solution-growth techniques for p-TCO thin films and powders. (A) Sol−gel and nitrate process for Cu−Al−O thin films (after Ref. [194]). (B) Spin-coating process for Ni−Co−O thin films from nitrate and organic precursors (after Ref. [115]). (C) Wet-chemical dip-coating process for CuAlO$_2$ thin films (after Ref. [198]). (D) Hydrothermal process for CuAlO$_2$ and CuAlO$_2$:Ga solid solutions (after Ref. [109]).

Table 6
Optical and electrical properties of $CuAlO_2$ thin films synthesized by various growth techniques

Growth technique	Thickness (nm)	Average visible transmittance (%)	Room-temperature conductivity (S cm^{-1})	E_a (meV)	Carrier concentration (cm^{-3})	Room-temperature Seebeck coefficient (μV K^{-1})	Reference	Remarks
PLD	500	70	0.095	∼200	1.3×10^{17}	+183	63	—
PLD	230	80	0.34	220	2.7×10^{19}	+214	78	Films were post-annealed in O$_2$ atmosphere (1.3 Pa)
r.f. sputtering	180	85	—	—	—	—	176	Preliminary Hall and TEP measurements confirmed p-type conductivity
d.c. sputtering	500–700	80	0.08	260	3.7×10^{17}	+128	178,196	Films were post-annealed in O$_2$ atmosphere (20 Pa) for 60 min
d.c. sputtering	500	85	0.39	196	1.2×10^{18}	+213	197	Films were post-annealed in O$_2$ atmosphere (20 Pa) for 90 min
r.f. magnetron reactive co-sputtering	250	20–80	—	—	—	—	179	Small amount of CuO was present in the film
Reactive d.c. sputtering	400–800	50–60	0.01–0.1	—	—	—	180	With facing metal targets and rotating substrate. Films were annealed at 1050 °C in N$_2$ atmosphere
Reactive d.c. sputtering	500	85	0.22	250	4.4×10^{17}	+115	181	Target was Cu + Al metal powder pellets
MOCVD	250	40	2	120	2.6×10^{19}	—	183	The films were a mixture of CuAlO$_2$, Cu$_2$O and CuAl$_2$O$_4$
PE-MOCVD	120	40	17.08	32	1.17×10^{20}	—	182	For those samples annealed in air for 5 min (at 350 °C)
Dip-coating	1000	—	5×10^{-3}	—	—	—	194	Results given for films deposited via nitrate route
Dip-coating	3500	90	—	—	—	—	198	Films were annealed in air (at 500 °C) for 180 min

Table 7
Optical and electrical properties of different delafossite p-TCO thin films synthesized by various growth techniques

Material	Method	Thickness (nm)	Average visible transmittance (%)	Room-temperature conductivity (S cm^{-1})	E_a (meV)	Carrier concentration (cm^{-3})	Room-temperature Seebeck coefficient (μV K^{-1})	Reference	Remarks
CuGaO$_2$	PLD	500	80	0.063	—	1.7×10^{18}	+560	87	—
CuGaO$_2$	Thermal co-evaporation	500	70−85	0.02	100	—	+360	66	Films were post-annealed in N$_2$ atmosphere at 800 °C for 90 min
CuGaO$_2$:Fe	r.f. sputtering	150	50−70	1.0	100	—	+500	66	Films were post-annealed in N$_2$ atmosphere at 800 °C for 90 min and 50% Ga replaced by Fe
CuInO$_2$:Ca	PLD	170	70	0.003	190	—	+480	88	7% Ca doped in place of In
CuScO$_2$	PLD	—	75−85	1.16×10^{-4}	—	—		177	Small amounts of Sc$_2$O$_3$, Cu$_2$O, Cu and CuO were present in the film
CuScO$_2$	r.f. sputtering	110	40	30.0	110	—	—	94	Actual formula was given as CuScO$_{2+y}$
CuScO$_2$:Mg	r.f. sputtering	250	15	20.0	95	—	—	66	5% Mg doping for Sc and the variation in σ_{RT} and T was due to change in post-deposition O$_2$ annealing press (133−10^7 Pa)
			70	0.08	—	—	—	66	
CuCrO$_2$	r.f. sputtering	200−300	30	1.0	—	—	—	66,95	—
CuCrO$_2$:Mg	r.f. sputtering	200−300	30−40	220	20[a]	—	+150	66,95	5% Cr replaced by Mg
CuYO$_2$	Co-evaporation	200	60	<0.02	—	—	—	66,96	—
CuYO$_2$:Ca	Co-evaporation	240	50	1.0	130	—	+275	66,96	1−2% Ca in Y site
CuNi$_{0.67}$Sb$_{0.3}$O$_2$:Sn	r.f. sputtering	150−200	60	0.05	170	—	+250	66,68	10% Sb replaced by Sn
AgCoO$_2$	r.f. sputtering	150	40−60	0.2	70	—	+220	66	Ag:Co = 1.1:1.0

[a] For low value of E_a, the word 'activation' should be used with caution.

Table 8
Optical and electrical properties of non-delafossite p-TCO thin films synthesized by various growth techniques

Material	Method	Thickness (nm)	Average visible transmittance (%)	Room-temperature conductivity (S cm^{-1})	E_a (meV)	Carrier concentration (cm^{-3})	Room-temperature Seebeck coefficient (μV K^{-1})	Reference	Remarks
SrCu$_2$O$_2$	PLD	150	70	3.9×10^{-3}	200	—	+260	112	—
SrCu$_2$O$_2$:K	PLD	120	80	4.83×10^{-2}	100	6.1×10^{17}	+260	70,112	3 at% Sr is replaced by K
SrCu$_2$O$_2$	e-beam evaporation	—	60	0.03	—	7.19×10^{16}	—	188	The film is a mixture of SrCu$_2$O$_2$, CuO and Cu$_2$O
NiCo$_2$O$_4$	r.f. sputtering	100	80	330	???	???	???	117	Co/(Co + Ni) = 0.67
NiCo$_2$O$_4$	Spin-coating	100	60	16.67	—	$<10^{16}$	—	115	Co/(Co + Ni) = 0.67
(LaO)CuS	r.f. sputtering	150	65	6.4×10^{-5}	240	2×10^{15}	+713	119,126	—
(LaO)CuS	R-SPE	150	—	0.66	—	1×10^{19}	+250	128,187	Large variation in the σ_{RT} was observed due to the change in the annealing atmosphere
(La$_{1-x}$Sr$_x$O) CuS	r.f. sputtering	150	60	20.0	—	2.7×10^{20}	+44	119,126	x = 0.03, and degenerate conductivity was observed
(LaO)CuS$_{1-x}$ Se$_x$	R-SPE	150	—	20.0	—	2×10^{19}	+200	128	x = 0.4
(LaO)CuSe	R-SPE	150	—	24.0	—	2×10^{19}	+250	128	—
(LaO)CuSe:Mg	R-SPE	150	—	140.0	—	2.2×10^{20}	—	128	20% La replaced by Mg and it showed degenerate p-type conductivity
In$_2$O$_3$−Ag$_2$O	r.f. magnetron sputtering	300	20	114	—	4.2×10^{19}	—	137	50 wt% Ag$_2$O content in the film
NiO	r.f. magnetron sputtering	120	40	7.14	—	1.3×10^{19}	—	65	—
ZnO	Reactive r.f. magnetron sputtering	5000	—	0.033	—	5×10^{15}	—	199	Sputtering gases were Ar + 83% O$_2$
ZnO:N	PLD with Ga and N co-doping	—	90	0.5	—	4×10^{19}	—	164	wt% of Ga$_2$O$_3$ in ZnO target was 0.1 and Ga:N dopant ratio was 1:2

ZnO:N	MBE	1900	–	0.025	240	9×10^{16}	–	160	Activation energy was estimated from PL results
ZnO:N	H$_2$O vapor assisted MO-MBE	1000	–	–		2.3×10^{15a}	–	161	
ZnO:N	MOCVD	600	–	0.01	–	1.7×10^{16}	–	159	NH$_3$ flux during deposition was 50 sccm
ZnO:As	r.f. magnetron sputtering	1500–2000	–	$\sim$1000	–	$\sim 1.0 \times 10^{17}$	–	198	Doping of As occurred from the diffusion of the GaAs (001) substrate. This was done by annealing the films at 600 °C for 1 h

^a This value is the net acceptor concentration obtained from C-V measurements.
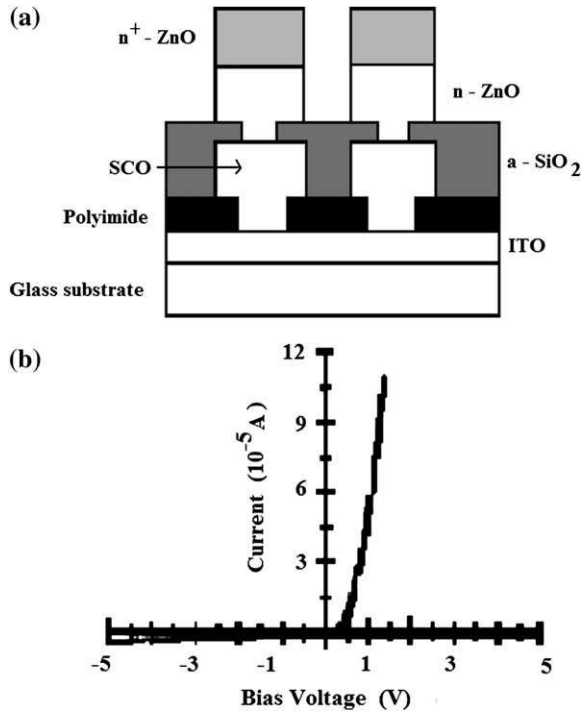
Fig. 44. (a) Structure of a transparent hetero-junction diode of the form: glass/ITO/p-SrCu$_2$O$_2$/n-ZnO/n$^+$-ZnO. ITO and n$^+$-ZnO are used as ohmic contacts (after Ref. [200]). (b) Rectifying $I-V$ characteristics of p—n hetero-junction as shown in Fig. 44(a) (after Ref. [200]).

exhibited by them and challenging problems thrown up for providing theoretical concepts in the physics associated with it [221—223]. Optical properties of nanocrystals are markedly related to their size and surface chemistry and drastically differ from those of bulk materials. Preparation and study of high quality quantum-dots [224], nanobelts [225] and nanowires [226] have been reported widely. These achievements in the last few years have focused nanoparticle research on their applications in electrical and optoelectronics devices [227,228].

Now, the synthesis and characterization of nanostructured n-TCOs are a very important and well-established field in nanotechnology and is still growing in stature. Therefore, the formation of nanocrystalline p-type counterpart may open up an extremely important and interesting field of research for the fabrication of all-transparent nanoactive devices. This will not only give a new dimension in the field of ''Transparent Electronics'', but new avenues may open up in the nano-particle research keeping an eye on its tremendous applications in optoelectronics technology.

As far as synthesis of nanocrystalline p-TCO thin film is concerned, Gong et al. [186] pre-pared an impure phase of copper aluminum oxide films by the chemical vapor deposition (CVD) method, which contained nanocrystalline phases of CuAlO$_2$ and Cu$_2$O. The particle size obtained by them was less than 10 nm. Also they have observed a blue-shift of the optical bandgap of the nanocrystalline films with respect to the bulk value. The same group also prepared nanostructured Cu—Al—O thin films (a mixture of CuAlO$_2$ and CuO) by reactive co-sputtering technique [182], with an average particle size around 40—60 nm and observed a similar blue-shift of the bandgap with a variation in the Cu:Al atomic ratio in their sample.

Fig. 45. (a) p−i−n structure composed of glass/n$^+$-ITO/i-ZnO/p$^+$-CuYO$_2$:Ca. Indium was used for ohmic contacts (after Ref. [205]). (b) Corresponding I−V curve of the above structure where ZnO layer is either undoped or Al-doped (after Ref. [205]).

It is well known that the quantum confinement effect put forward by Brus [220], is responsible for the bandgap widening of semiconductor nanocrystals, where the size dependency of the bandgap ($E_{g[nano]}$) is given by the following formula:

$$\Delta E = E_{g[nano]} - E_{g[bulk]} = \frac{h^2}{8\mu^*(r)^2} - \frac{1.8e^2}{(r)\varepsilon} \tag{3}$$

Fig. 46. I−V curve of p-CuYO$_2$:Ca/n-ZnO:Al transparent diode (after Ref. [96]).

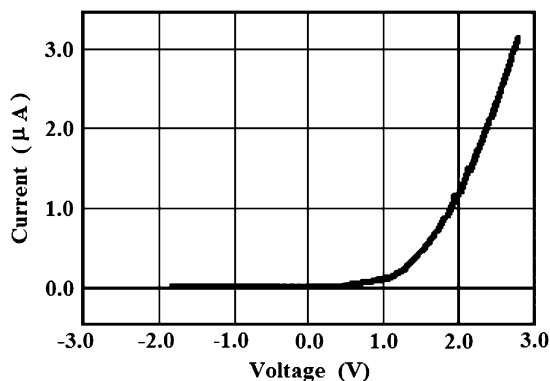Fig. 47. Optical transparency of n-ZnO/p-Cu−Al−O diode. Inset: corresponding diode structure (after Ref. [207]).

where ΔE is the shift of the bandgap with respect to the bulk bandgap $E_{g[bulk]}$, r is the radius of the nanoparticles, μ^* is the reduced mass of electron−hole effective masses and ε is the semi-conductor dielectric constant. The first term of the RHS expression in the equation represents the particle-in-a box quantum localization energy and has a $(1/r^2)$ dependence for both electron

Fig. 48. (a) All-delafossite p−n homo-junction diode of the form YSZ/ITO/p-CuInO$_2$:Ca/n-CuInO$_2$:Sn/ITO (after Ref. [89]). (b) $I-V$ characteristics of all-delafossite diode consists of p-CuInO$_2$:Ca/n-CuInO$_2$:Sn layers as shown in (a) (after Ref. [89]).

Fig. 49. $I-V$ characteristics of p-ZnO:As/n-ZnO:Al homo-junction. Inset: corresponding diode structure (after Ref. [198]).

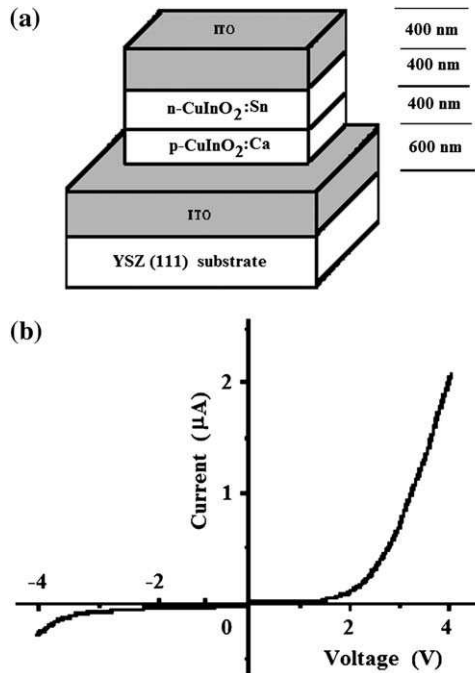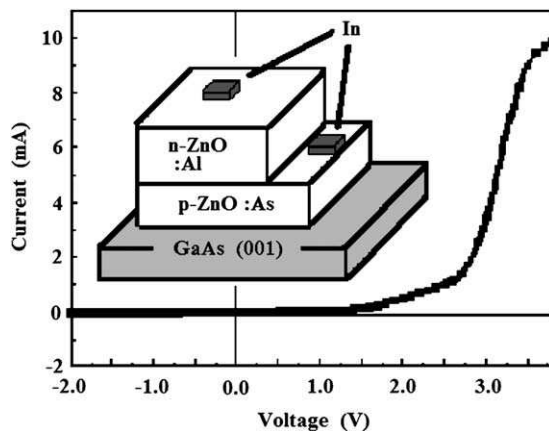and hole. The second term represents the Coulomb energy with a $(1/r)$ dependence. In the limit of large r, the value of $E_{g[nano]}$ approaches that of $E_{g[bulk]}$. But the observed blue-shift of the bandgap of nanocrystalline Cu−Al−O films prepared by Gong and co-authors [182,186], as mentioned above, may not be explained satisfactorily by Brus's theory of quantum confinement as the theory was developed for single-phase material. We have recently reported the synthesis of phase-pure $CuAlO_2$ nanoparticles by the d.c. sputtering technique [229] from sintered $CuAlO_2$ target. From the optical data we have observed a blue-shift or broadening of the bandgap of the material with decrease in the particle size, which may be attributed to the quantum confinement effect. The variation of the particle size was done by varying the deposition time, which ranges from 3 min to 150 min. The average particle size varies from 10 to 90 nm with increase in the deposition time, whereas the optical bandgap varies from 3.94 to 3.34 eV, respectively, in the above range.

Fig. 51(a) and (b) shows the XRD patterns of $CuAlO_2$ target and nanostructured films deposited for different deposition times, respectively. Fig. 52(a) and (b) shows the optical
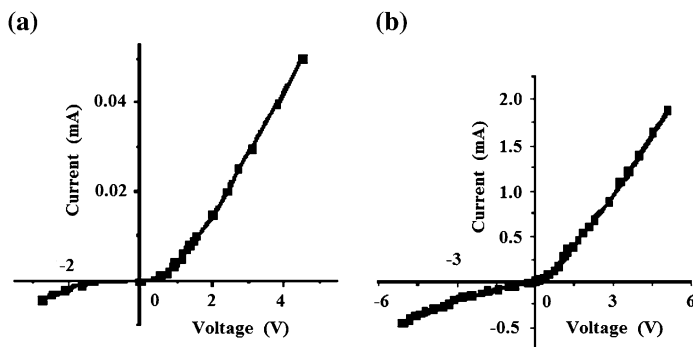

Fig. 50. $I-V$ characteristics of all-ZnO p−n homo-junctions (a) without annealing, and (b) after annealing (after Ref. [199]).

Table 9
Parameters of different all-transparent diodes

Diode structure		p-NiO/i-NiO/i-ZnO/n-ZnO:Al	n-ZnO/p-SrCu$_2$O$_2$	n-ZnO/p-SrCu$_2$O$_2$:K	n-ZnO:Al/p-CuYO$_2$:Ca	n-ZnO/p-CuAlO$_2$	n-CuInO$_2$:Sn/p-CuInO$_2$:Ca	n-ZnO:Al/p-ZnO:As	n-ZnO/p-ZnO
Thickness (nm)	p-layer	195	300	200	300	400	400	1500−2000	5000
	i-layer	216	–	–	–	–	–	–	–
	n-layer	400	300−1000	200	250	400	400	600	5000
Carrier concentration (cm^{-3})	p-layer	10^{19}	10^{17}	∼10^{18}	–	–	–	–	∼5 × 10^{15}
	n-layer	7 × 10^{20}	5 × 10^{18}	∼10^{18}	–	–	–	–	∼6 × 10^{15}
Substrate		Glass	Glass	YSZ (111)	Glass	Glass	YSZ (111)	GaAs (001)	Si (100)
Deposition technique	p-layer	r.f. magnetron sputtering	Reactive co-evaporation in O$_2$ atmosphere	PLD	Reactive co-evaporation in O$_2$ atmosphere	PLD	PLD	r.f. magnetron sputtering	r.f. magnetron reactive sputtering
	i-layer	r.f. magnetron sputtering with post-annealing in air (at 300 °C)	–	–	–	–	–	–	–
	n-layer	–	Magnetron sputtering	PLD	r.f. magnetron sputtering	PLD	PLD	r.f. magnetron sputtering	r.f. magnetron reactive sputtering
Electrodes	p-side	Al	ITO	Ni	In	ITO	ITO	In	Au/Al
	n-side	Al	n$^+$-ZnO	ITO	ITO	n$^+$-ZnO	ITO	In	Au/Al
Turn-on voltage (V)		∼1.5	∼0.5	∼1.0	0.4−0.8	0.4−1.0	1.8	∼2.5	∼1.0
Diode factor		–	1.62	–	–	–	–	–	–
Reference		65	200	201	96	206	89	198	199
Remarks		The diode showed only 20% transparency in the visible region	The diode showed 70% to 80% transparency in the visible region	UV emission was observed when current was injected through the junction	The diode showed 40% transparency in the visible region	n-ZnO layer grown at a temperature of more than 250 °C showed good rectifying characteristics	The diode showed 60% to 80% transparency in the visible region	p-layer was obtained by vacuum-annealing the as-deposited film at 600 °C	p-type and n-type layers were obtained for Ar + 83% O$_2$ and Ar + 50% O$_2$ sputtering atmosphere, respectively

Table 10
Different growth techniques and parameters of TFETs

Active channel	Gate insulator	Gate electrode	Substrate used	Mobility ($cm^2 V^{-1} s^{-1}$)	On/off ratio	Visible transparency (%)	Reference
SnO$_2$:Sb (thickness ∼110 nm) (deposition technique: PLD)	PbZr$_{0.2}$Ti$_{0.8}$O$_3$ (thickness ∼160 nm) (deposition technique: PLD)	SrRuO$_3$ (thickness ∼140 nm) (deposition technique: PLD)	SrTiO$_3$ (100)	10.0	∼10^4	Transparent, as seen in the figure provided, but no numerical data given	212[a], 213
ZnO (thickness ∼100 nm) (deposition technique: PLD)	Al$_2$O$_3$ + TiO$_2$[b] (thickness ∼220 nm) (deposition technique: ALD)	ITO (thickness ∼200 nm) (deposition technique: sputtering)	Glass	2.5	∼10^7	75	214
ZnO (thickness ∼140 nm) (deposition technique: PLD)	SiO$_2$ + SiN$_x$[c] (thickness ∼250 and 50 nm, respectively) (deposition technique: PECVD)	ITO (thickness ∼100 nm) (deposition technique: e-beam evaporation)	Glass	1	10^5	80	215
InGaO$_3$(ZnO)$_5$[d] (thickness ∼120 nm) (deposition technique: PLD)	a-HfO$_2$ (thickness ∼80 nm) (deposition technique: PLD)	ITO (thickness ∼30 nm) (deposition technique: PLD)	YSZ (111)	80	∼10^6	80	217[e]

[a] Due to the presence of ferroelectric insulator PbZr$_{0.2}$Ti$_{0.8}$O$_3$, the device showed intrinsic memory function.
[b] Al$_2$O$_3$ + TiO$_2$ is alternative layers of Al$_2$O$_3$ and TiO$_2$.
[c] This TFET has a double layer Gate insulator.
[d] Single-crystalline InGaO$_3$(ZnO)$_5$ is used as active channel layer.
[e] The device has top-gate structure.

Fig. 51. (a) XRD pattern of CuAlO$_2$ powder (after Ref. [221]). (b) XRD pattern of nanocrystalline CuAlO$_2$ thin film deposited for (#1) 15 min and (#2) 45 min (after Ref. [221]).

transmission spectra and direct bandgap values of nanocrystalline CuAlO$_2$ thin films with different deposition times.

8. Conclusions

(1) A comprehensive and up-to-date picture of recent developments in the field of transparent p-type semiconducting oxide thin film technology has been reported. The use of non-stoichiometry and various dopings for p-TCO thin films by different methods has been reported. With better understanding of the defect chemistry and the role of dopants to increase the hole conductivity of these materials, newer and higher quality p-TCO thin films can be developed for better device applications.

Fig. 52. (a) Optical transmission spectra of nanocrystalline CuAlO$_2$ thin films with different deposition times (after Ref. [221]). (b) Determination of bandgap of nanocrystalline CuAlO$_2$ films (after Ref. [221]).

(2) Although various models such as ''CMVB'', ''co-doping'' etc. have been proposed to obtain new types of p-TCO thin films and a large number of deposition techniques have been adopted with widely varying growth parameters to fabricate new p-TCO thin films with better electrical and optical properties the maximum conductivity obtained for p-TCO thin films are still one or two orders of magnitude less than the corresponding best n-TCO thin films. Increasing the conductivity of p-TCO thin films without sacrificing their visible transmittance is the most significant challenge for p-TCO technology in order to obtain high performance active devices suitable for ''Invisible Electronics''.

(3) Development of delafossite thin films with both types of conductivity is another most interesting field of research to obtain high quality junction devices. With the newer methods of material syntheses, developing rapidly in thin film technology, fabrication of

all-delafossite transparent diodes may not remain a hard task. Similarly, the renaissance of ZnO thin films has already begun with the development of p-type ZnO thin films. The selection of the proper growth parameters and hence reproducibility of these films may revolutionize p-TCO technology in the near future. The achievement of high mobility TFETs is another important step towards the goal of ''Transparent Electronics''.

(4) In the fast growing field of nanotechnology, nanostructured p-TCO thin films may open up an extremely important and interesting field of research for the fabrication of all-transparent nanoactive devices. This will give an added impetus in the field of ''Transparent Electronics'' and new avenues may open up in the nanoparticle research which could offer tremendous applications in optoelectronics technology.

Acknowledgement

References

[1] K. Badekar, Ann. Phys. (Leipzig) 22 (1907) 749.
[2] C.M. Lampert, Sol. Energy Mater. 6 (1981) 1.
[3] K.L. Chopra, S. Major, D.K. Pandya, Thin Solid Films 102 (1983) 1.
[4] I. Hamberg, C.G. Granqvist, J. Appl. Phys. 60 (1986) R123.
[5] L. Holland, Vacuum Deposition of Thin Films, Wiley, New York, 1958.
[6] H. Cachet, A. Gamard, G. Campet, B. Jousseaume, T. Toupance, Thin Solid Films 388 (2001) 41.
[7] R. Wendt, K. Ellmer, Surf. Coat. Technol. 93 (1997) 27.
[8] H.L. Hartnagel, A.L. Dawar, A.K. Jain, C. Jagadish, Semiconducting Transparent Thin Films, IOP Publishing Ltd., Bristol and Philadelphia, 1995.
[9] D.S. Ginley, C. Bright, MRS Bull. (August 2000) 15.
[10] R.J. Cava, J.M. Philips, J. Kwo, G.A. Thomas, R.B. van Dover, S.A. Carter, J.J. Krajewski, W.F. Peck Jr., J.H. Marshall, D.H. Rapkin, Appl. Phys. Lett. 64 (1994) 2071.
[11] J.M. Philips, R.J. Cava, G.A. Thomas, S.A. Carter, J. Kwo, T. Siegrist, J.J. Krajewski, J.H. Marshall, W.F. Peck Jr., D.H. Rapkine, Appl. Phys. Lett. 67 (1995) 2246.
[12] A.J. Freeman, K.R. Poeppelmeier, T.O. Mason, R.P.H. Chang, T.J. Marks, MRS Bull. (August 2000) 45.
[13] R.G. Gordon, MRS Bull. (August 2000) 52.
[14] J.M. Mochel, U.S. Patent No. 2,564,706, 1947.
[15] W.R. Sinclair, F.G. Peters, D.W. Stillinger, S.E. Koonce, J. Electrochem. Soc. 112 (1965) 1096.
[16] W.O. Lytle, A.E. Junge, U.S. Patent No. 2,566,346, 1951.
[17] R.G. Gordon, U.S. Patent No. 4,146,657, 1979.
[18] A.N. Banerjee, S. Kundoo, P. Saha, K.K. Chattopadhyay, J. Sol–Gel Sci. Technol. 28 (2003) 105.
[19] A.N. Banerjee, R. Maity, S. Kundoo, K.K. Chattopadhyay, Phys. Status Solidi A 201 (2004) 983.
[20] S. Major, A. Banerjee, K.L. Chopra, Thin Solid Films 122 (1984) 31.
[21] T. Minami, H. Nanto, S. Takata, Jpn. J. Appl. Phys., Part 2: Lett. 23 (1984) L280.
[22] J. Hu, R.G. Gordon, Sol. Cells 30 (1991) 437.
[23] P.S. Vijayakumar, K.A. Blaker, R.D. Welting, B. Wong, A.T. Halani, C. Park, U.S. Patent No. 4,751,149, 1988.
[24] B.H. Choi, H.B. Im, J.S. Song, K.H. Yoon, Thin Solid Films 193 (1990) 712.
[25] J. Hu, R.G. Gordon, J. Appl. Phys. 72 (1992) 5381.
[26] J.M. Mochel, U.S. Patent No. 2,564,707, 1951.
[27] L. Holland, G. Siddall, Vacuum III (1955).
[28] J.N. Avaritsiotis, R.P. Howson, Thin Solid Films 77 (1981) 351.

[29] R. Groth, Phys. Status. Solidi 14 (1966) 69.

[30] A.J. Nozik, U.S. Patent No. 3,811,953, 1974.

[31] G. Haacke, W.E. Mealmaker, L.A. Siegel, Thin Solid Films 55 (1978) 67.

[32] J.L. Vossen, RCA Rev. 32 (1971) 269.

[33] H. Enoki, T. Nakayama, J. Echigoya, Phys. Status Solidi A 129 (1992) 181.

[34] T. Minami, H. Sonohara, S. Takata, H. Sato, Jpn. J. Appl. Phys., Part 2: Lett. 33 (1994) L1693.

[35] R.J. Cava, S.Y. Hou, J.J. Krajewski, J.H. Marshall, W.F. Pack, D.H. Rapkin, R.B. van Dover, Appl. Phys. Lett. 65 (1994) 115.

[36] T. Otabe, K. Ueda, A. Kudoh, H. Hosono, H. Kawazoe, Appl. Phys. Lett. 72 (1998) 1036.

[37] S.E. Dali, M. Jayachandran, M.J. Chockalingam, J. Mater. Sci. Lett. 18 (1999) 915.

[38] D.D. Edwards, T.O. Mason, F. Goutenoire, K.R. Poeppelmeier, Appl. Phys. Lett. 70 (1997) 1706.

[39] T. Minami, S. Takata, T. Kakumu, H. Sonohara, Thin Solid Films 270 (1995) 22.

[40] T. Minami, T. Kakumu, K. Shimokawa, S. Takata, Thin Solid Films 317 (1998) 318.

[41] T. Omata, N. Ueda, K. Ueda, H. Kawazoe, Appl. Phys. Lett. 64 (1994) 1077.

[42] D.R. Kammler, T.O. Mason, D.L. Young, T.J. Coutts, J. Appl. Phys. 90 (2001) 3263.

[43] T. Minami, MRS Bull. (August 2000) 38.

[44] B.G. Lewis, D.C. Paine, MRS Bull. (August 2000) 22.

[45] C.G. Granqvist, A. Azens, A. Hjelm, L. Kullman, G.A. Niklasson, D. Ronnow, M.S. Mattson, M. Veszelei, G. Vaivars, Sol. Energy 63 (1998) 199.

[46] D.R. Kammler, D.D. Edwards, B.J. Ingram, T.O. Mason, G.B. Palmer, A. Ambrosini, K.R. Poeppelmeier, in: V.K. Kapur, R.D. McConnel, D. Carlson, G.P. Ceasan, A. Rohatgi (Eds.), Photovoltaics for the 21st Century. The Electrochemical Society Proceedings, Pennington NJ, 99-11, 1999, p. 68.

[47] S.H. Lee, K.H. Hwang, S.K. Joo, in: K.C. Ho, D.A. McArthur (Eds.), Electrochromic Materials, Second International Symposium, The Electrochemical Society Proceedings, Pennington NJ, 94-2, 1994, p. 290.

[48] P.S. Lugg, S. Bommarito, J. Bailey, K. Budd, P. Cullen, K. Chen, L.C. Hardy, M. Nachbor, in: Solid State Ionic Devices, The Electrochemical Society Proceedings, Pennington NJ, 99-13, 1999, p. 284.

[49] Y. Nakato, K.I. Kai, K. Kawabe, Sol. Energy Mater. Sol. Cells 37 (1995) 323.

[50] T.T. Emons, J. Li, L.F. Nazar, J. Am. Chem. Soc. 124 (2002) 8517.

[51] M.G. Hutchins, G.D. McMeeking, Biosensor Patent No. 90,27,607.2, 1990.

[52] Y. He, J. Kanicki, Appl. Phys. Lett. 76 (2000) 661.

[53] J.F. Wager, Science 300 (2003) 1245.

[54] C.M. Lampert, Sol. Energy Mater. 21 (1990) 191.

[55] C. Grivas, S. Mallis, L. Boutsikaris, D.S. Gill, N.A. Vainos, P.J. Chandler, Laser Phys. 8 (1998) 326.

[56] K. Moschovis, E. Gagaoudakis, E. Chatzitheodoridis, G. Kiriakidis, S. Mailis, E. Tzamali, N.A. Vainos, H. Fritzsche, Appl. Phys. A 66 (1998) 651.

[57] S. Moller, C. Perlov, W. Jackson, C. Taussig, S.R. Forest, Nature 426 (2003) 166.

[58] R.A. Hayes, B.J. Feenstra, Nature 425 (2003) 1038.

[59] R.L. Cornia, J.B. Fenn, H. Memarian, R. Ringer, Proceedings of 41st Annual Technical Conference, Boston, SVC, 1998, p. 452.

[60] D.R. Cairns, R.P. Witte, D.K. Sparacin, S.M. Sachsman, D.C. Paine, G.P. Crawford, R. Newton, Appl. Phys. Lett. 76 (2000) 1425.

[61] C.H. Seager, D.C. McIntyre, W.L. Warren, B.A. Tuttle, Appl. Phys. Lett. 68 (1996) 2660.

[62] M.W.J. Prince, K.O. Gross-Holtz, G. Muller, J.B. Cillessen, J.B. Giesbers, R.P. Weening, R.M. Wolf, Appl. Phys. Lett. 68 (1996) 3650.

[63] H. Kawazoe, M. Yasukawa, H. Hyodo, M. Kurita, H. Yanagi, H. Hosono, Nature 389 (1997) 939.

[64] G. Thomas, Nature 389 (1997) 907.

[65] H. Sato, T. Minami, S. Takata, T. Yamada, Thin Solid Films 236 (1993) 27.

[66] J. Tate, M.K. Jayaraj, A.D. Draeseke, T. Ulbrich, A.W. Sleight, K.A. Vanaja, R. Nagarajan, J.F. Wager, R.L. Hoffman, Thin Solid Films 411 (2002) 119.

[67] R. Nagarajan, N. Duan, M.K. Jayaraj, J. Li, K.A. Vanaja, A. Yokochi, A. Draeseke, J. Tate, A.W. Sleight, Int. J. Inorg. Mater. 3 (2001) 265.

[68] R. Nagarajan, S. Uma, M.K. Jayaraj, J. Tate, A.W. Sleight, Solid State Sci. 4 (2002) 787.

[69] D.P. Norton, Mater. Sci. Eng. R. 43 (2004) 139.

[70] H. Kawazoe, H. Yanagi, K. Ueda, H. Hosono, MRS Bull. (August 2000) 28.

[71] S. Fraga, S. Karwowski, K.M.S. Saxena, Handbook of Atomic Data, Elsevier, Amsterdam, 1976.

[72] D. DeVault, J. Chem. Educ. 21 (1944) 526.

[73] J.C. Bailar Jr., H.J. Eméleus, Sir N. Ronald, A.F. Trotman-Dickenson (Eds.), Comprehensive Inorganic Chemistry, Pergamon, New York, NY, 1973.

[74] Y.K. Leung, A.K. Khan, J.F. Kos, F.P. Koffyberg, Proceedings of National Conference on Solar Energy, Montreal, Solar Energy Society of Canada, 1981, p. 124.

[75] J.P. Dahl, A.C. Switendick, J. Phys. Chem. Solids 27 (1966) 931.

[76] M. Hayashi, K. Katsuki, J. Phys. Soc. Jpn. 5 (1950) 380.

[77] L. Kleinman, K. Mednick, Phys. Rev. B 21 (1980) 1549.

[78] H. Yanagi, S. Inoue, K. Ueda, H. Kawazoe, H. Hosono, N. Hamada, J. Appl. Phys. 88 (2000) 4159.

[79] R.D. Shannon, D.B. Rogers, C.T. Prewitt, Inorg. Chem. 10 (1971) 713.

[80] C.T. Prewitt, R.D. Shannon, D.B. Rogers, Inorg. Chem. 10 (1971) 719.

[81] D.B. Rogers, R.D. Shannon, C.T. Prewitt, J.L. Gilson, Inorg. Chem. 10 (1971) 723.

[82] H. Hahn, C. Lorent, Z. Anorg. Allg. Chem. 279 (1955) 281.

[83] F.A. Benko, F.P. Koffyberg, J. Phys. Chem. Solids 45 (1984) 57.

[84] T. Ishiguro, A. Kitazawa, N. Mizutani, M. Kato, J. Solid State Chem. 40 (1981) 170.

[85] T. Ishiguro, N. Ishizawa, N. Mizutani, M. Kato, J. Solid State Chem. 41 (1982) 132.

[86] T. Ishiguro, N. Ishizawa, N. Mizutani, M. Kato, Acta. Crystallogr. B39 (1983) 564.

[87] K. Ueda, T. Hase, H. Yanagi, H. Kawazoe, H. Hosono, H. Ohta, M. Orita, M. Hirano, J. Appl. Phys. 89 (2001) 1790.

[88] H. Yanagi, T. Hase, S. Ibuki, K. Ueda, H. Hosono, Appl. Phys. Lett. 78 (2001) 1583.

[89] H. Yanagi, K. Ueda, H. Ohta, M. Orita, M. Hirano, H. Hosono, Solid State Commun. 121 (2001) 15.

[90] B.V. Kohler, M. Jansen, Z. Anorg. Allg. Chem. 543 (1986) 73.

[91] M. Shimode, M. Sasaki, K. Mukaida, J. Solid State Chem. 151 (2000) 16.

[92] J. Robertson, P.W. Peacock, M.D. Towler, R. Needs, Thin Solid Films 411 (2002) 96.

[93] B.J. Ingram, T.O. Mason, R. Asahi, K.T. Park, A.J. Freeman, Phys. Rev. B 64 (2001) 155114.

[94] N. Duan, A.W. Sleight, M.K. Jayaraj, J. Tate, Appl. Phys. Lett. 77 (2000) 1325.

[95] R. Nagarajan, A.D. Draeseke, A.W. Sleight, J. Tate, J. Appl. Phys. 89 (2001) 8022.

[96] M.K. Jayaraj, A.D. Draeseke, J. Tate, A.W. Sleight, Thin Solid Films 397 (2001) 244.

[97] L.F. Mattheiss, Phys. Rev. B 48 (1993) 18300.

[98] O. Crottaz, F. Kubel, H. Schmid, J. Solid State Chem. 122 (1996) 247.

[99] Y.J. Shin, J.H. Kwak, S. Yoon, Bull. Korean Chem. Soc. 18 (1997) 775.

[100] J.-S. Kang, J.H. Kwak, Y.J. Shin, S.W. Han, K.H. Kim, B.I. Min, Phys. Rev. B 61 (2000), 10682.

[101] H.C. Kandpal, R. Seshadri, Solid State Sci. 4 (2002) 1045.

[102] P. Kofstad, Nonstoichiometry, Diffusion, and Electrical Conductivity in Binary Metal Oxides, Wiley-Interscience, New York, NY, 1972.

[103] K. Koumoto, H. Koduka, W.S. Seo, J. Mater. Chem. 11 (2001) 251.

[104] R.J. Cava, W.F. Peck Jr., J.J. Krajewski, S.W. Cheong, H.Y. Hwang, J. Mater. Res. 9 (1994) 314.

[105] R.J. Cava, H.W. Zandbergen, A.P. Ramirez, H. Tagaki, C.T. Chien, J.J. Krajewski, W.F. Peck Jr., J.V. Waszczak, G. Meigs, R.S. Roth, L.F. Schneemeyer, J. Solid State Chem. 104 (1993) 437.

[106] M.K. Jayaraj, A. Draeseke, J. Tate, N. Duan, A.W. Sleight, Proceedings of the MRS Workshop on Transparent Conductive Oxide, Denever, CO, 2000.

[107] M.V. Lalić, J.M. Filho, A.W. Carbonari, R.N. Saxena, M. Moralles, J. Phys.: Condens. Matter 14 (2002) 5517.

[108] M.V. Lalić, J.M. Filho, A.W. Carbonari, R.N. Saxena, Solid State Commun. 125 (2003) 175.

[109] D.Y. Shahriari, A. Barnabè, T.O. Mason, K.R. Poeppelmeier, Inorg. Chem. 40 (2001) 5734.

[110] F.A. Benko, F.P. Koffyberg, J. Phys. Chem. Solids 48 (1987) 431.

[111] H. Yanagi, S. Park, A.D. Draeseke, D.A. Keszler, J. Tate, J. Solid State Chem. 175 (2003) 34.

[112] A. Kudo, H. Yanagi, H. Hosono, H. Kawazoe, Appl. Phys. Lett. 73 (1998) 220.

[113] C.L. Teske, H. Müller-Buschbaum, Z. Anorg. Allg. Chem. 379 (1970) 113.

[114] S. Boudin, C. Felser, F. Studer, Solid State Sci. 5 (2003) 741.

[115] C.F. Windisch Jr., K.M. Ferris, G.J. Exarhos, J. Vac. Sci. Technol. A 19 (2001) 1647.

[116] J.A.K. Tareen, A. Malecki, J.P. Doumerc, J.C. Launay, P. Dordor, M. Pouchard, P. Hagenmuller, Mater. Res. Bull. 19 (1984) 989.

[117] C.F. Windisch Jr., M.H. Engelhard, D.C. Stewart, Thin Solid Films 398−399 (2001) 45.

[118] K. Ueda, S. Inoue, S. Hirose, H. Kawazoe, H. Hosono, Appl. Phys. Lett. 77 (2000) 2701.

[119] H. Hiramatsu, K. Ueda, H. Ohta, M. Orita, M. Hirano, H. Hosono, Thin Solid Films 411 (2002) 125.

[120] M. Palazzi, C.R. Acad. Sci. Paris, 292 (1981) 789.

[121] K. Ishikawa, S. Kinosita, Y. Suzuki, S. Matsuura, T. Nakanishi, M. Aizawa, Y. Suzuki, J. Electrochem. Soc. 138 (1991) 1166.

[122] Y. Takano, K.-I. Yahagi, K. Sekizawa, Physica B 206 & 207 (1995) 764.

[123] K. Ueda, S. Inoue, H. Hosono, N. Sarukura, M. Hirano, Appl. Phys. Lett. 78 (2001) 2333.

[124] K. Ueda, H. Hosono, J. Appl. Phys. 91 (2002) 4768.

[125] K. Takase, M. Koyano, T. Shimizu, K. Makihara, Y. Takahashi, Y. Takano, K. Sekizawa, Solid State Commun. 123 (2002) 531.

[126] H. Hiramatsu, M. Orita, M. Hirano, K. Ueda, H. Hosono, J. Appl. Phys. 91 (2002) 9177.

[127] H. Hiramatsu, K. Ueda, K. Takafuji, H. Ohta, M. Orita, M. Hirano, T. Kamiya, H. Hosono, J. Appl. Phys. 94 (2003) 5805.

[128] H. Hiramatsu, K. Ueda, H. Ohta, M. Hirano, T. Kamiya, H. Hosono, Appl. Phys. Lett. 82 (2003) 1048.

[129] K. Ueda, H. Hiramatsu, H. Ohta, M. Hirano, T. Kamiya, H. Hosono, Phys. Rev. B 69 (2004) 155305.

[130] K. Ueda, H. Hosono, Thin Solid Films 411 (2002) 115.

[131] W.J. Zhu, Y.Z. Huang, C. Dong, Z.X. Zhao, Mater. Res. Bull. 29 (1994) 143.

[132] S.-I. Inoue, K. Ueda, H. Hosono, N. Hamada, Phys. Rev. B 64 (2001) 245211.

[133] Y. Furukawa, S. Ikeda, K. Kumagai, K. Mori, Y. Takano, K. Sekizawa, Phys. Rev. B 62 (2000) 15598.

[134] Y. Takano, K. Mori, K. Koizumi, H. Ozaki, K. Sekizawa, J. Alloys Compd. 275–277 (1998) 447.

[135] K. Sekizawa, Y. Takano, K. Mori, T. Yahagi, Czech. J. Phys. 46 (1996) 1943.

[136] M. Palazzi, C. Carcaly, J. Flahaut, J. Solid State Chem. 35 (1980) 150.

[137] T. Minami, T. Shimokawa, T. Miyata, J. Vac. Sci. Technol. A 16 (1998) 1218.

[138] E. Fortiu, F.L. Weichman, Phys. Status Solidi A 5 (1964) 515.

[139] A.B. Kunz, J. Phys. C 14L (1981) 445.

[140] D. Adler, J. Feinleib, Phys. Rev. B 2 (1970) 3112.

[141] P. Lunkenheimer, A. Loidl, C.R. Ottermann, K. Bange, Phys. Rev. B 44 (1991) 5927.

[142] E. Antolini, J. Mater. Sci. 27 (1992) 3335.

[143] G.A. Slack, J. Appl. Phys. 31 (1960) 1571.

[144] M.R. Norman, Phys. Rev. Lett. 64 (1990) 1162.

[145] I.G. Austin, N.F. Mott, Adv. Phys. 18 (1969) 41.

[146] A.J. Bosman, H.J. van Daal, Adv. Phys. 19 (1970) 1.

[147] J.S.E.M. Svensson, C.G. Granqvist, Appl. Phys. Lett. 49 (1986) 1566.

[148] S. Yamada, T. Yoshioka, M. Miyashita, K. Urabe, M. Kitao, J. Appl. Phys. 63 (1988) 2116.

[149] K. Bange, T. Gambke, Adv. Mater. 2 (1990) 10.

[150] D.A. Wruck, M.A. Dixon, M. Rubin, S.N. Bogy, J. Vac. Sci. Technol. A 9 (1991) 2170.

[151] S.I. Cordoba-Torresi, C. Gabrielli, A. Hugot-Le Goff, R. Torresi, J. Electrochem. Soc. 138 (1991) 1548.

[152] S.I. Cordoba-Torresi, A. Hugot-Le Goff, S. Joiret, J. Electrochem. Soc. 138 (1991) 1554.

[153] D.G. Thomas, J. Phys. Chem. Solids 9 (1959) 31.

[154] J.J. Lander, J. Phys. Chem. Solids 15 (1960) 324.

[155] K. Hümmer, Phys. Status Solidi B 56 (1973) 249.

[156] Y. Sato, S. Sato, Thin Solid Films 281–282 (1996) 445.

[157] K. Minegishi, Y. Koiwai, Y. Kikuchi, K. Yano, M. Kasuga, A. Shimizu, Jpn. J. Appl. Phys. 36 (1997) L1453.

[158] X.-L. Guo, H. Tabata, T. Kawai, J. Cryst. Growth 233 (2001) 135.

[159] J. Wang, G. Du, B. Zhao, X. Yang, Y. Zhang, Y. Ma, D. Liu, Y. Chang, H. Wang, H. Yang, S. Yang, J. Cryst. Growth 255 (2003) 293.

[160] D.C. Look, D.C. Reynolds, C.W. Litton, R.L. Jones, D.B. Eason, G. Cantwell, Appl. Phys. Lett. 81 (2002) 1830.

[161] A.B.M.A. Ashrafi, I. Suemune, H. Kumano, S. Tanaka, Jpn. J. Appl. Phys. 41 (2002) L1281.

[162] Y.R. Ryu, S. Zhu, D.C. Look, J.M. Wrobel, H.M. Joeng, H.W. White, J. Cryst. Growth 216 (2000) 330.

[163] T. Yamamoto, H.K. Yoshida, Jpn. J. Appl. Phys. 38 (1999) L166.

[164] M. Joseph, H. Tabata, T. Kawai, Jpn. J. Appl. Phys. 38 (1999) L2505.

[165] K. Tamura, T. Makino, A. Tsukazaki, M. Sumiya, S. Fuke, T. Furumochi, M. Lippmaa, C.H. Chia, Y. Segawa, H. Koinuma, M. Kawasaki, Solid State Commun. 127 (2003) 265.

[166] K. Nakahara, H. Takasu, P. Fons, A. Yamada, K. Iwata, K. Matsubara, R. Hunger, S. Niki, Appl. Phys. Lett. 79 (2001) 4139.

[167a] A. Tsukazaki, H. Saito, K. Tamura, M. Ohtani, H. Koinuma, M. Sumiya, S. Fuke, T. Fukumura, M. Kawasaki, Appl. Phys. Lett. 81 (2002) 235.

[167b] R. Triboulet, J. Perrière, Prog. Cryst. Growth Charact. Mater. 47 (2003) 65.

[168] S. Park, D.A. Keszlor, M.M. Valencia, R.L. Hoffman, J.P. Bender, J.F. Wager, Appl. Phys. Lett. 80 (2002) 4393.

[169] W.J. Wu, Y.Z. Huang, F. Wu, C. Dong, H. Chen, Z.X. Zhao, Mater. Res. Bull. 29 (1994) 505.

[170] H. Yanagi, S. Park, A.D. Draeseke, D.A. Keszler, J. Tate, J. Solid State Chem. 175 (2003) 34.

[171] J.E. Iglesias, K.E. Pachali, H. Stoinfink, J. Solid State Chem. 9 (1974) 6.

[172] L.I. Maissel, R. Glang, Handbook of Thin Films Technology, McGraw-Hill, New York, NY, 1970.

[173] D.B. Chrisey, G.K. Hubler, Pulsed Laser Deposition of Thin Films, Wiley-Interscience, New York, NY, 1994.

[174] K.L. Chopra, Thin Film Phenomena, McGraw-Hill, New York, NY, 1969.

[175] J.C. Anderson, The Use of Thin Films in Physical Investigations, Academic, New York, NY, 1966.

[176] R.E. Stauber, J.D. Perkins, P.A. Parilla, D.S. Ginley, Electrochem. Solid-State Lett. 2 (1999) 654.

[177] Y. Kakehi, S. Nakao, K. Satoh, T. Yotsuya, Thin Solid Films 445 (2003) 294.

[178] A.N. Banerjee, S. Kundoo, K.K. Chattopadhyay, Thin Solid Films 440 (2003) 5.

[179] A.N. Banerjee, K.K. Chattopadhyay, Appl. Surf. Sci. 225 (2004) 10.

[180] A.N. Banerjee, R. Maity, P.K. Ghosh, K.K. Chattopadhyay, Thin Solid Films 474 (2005) 261.

[181] A.N. Banerjee, C.K. Ghosh, K.K. Chattopadhyay, Sol. Energy Mater. Sol. Cells 89 (2005) 75.

[182] C.H. Ong, H. Gong, Thin Solid Films 445 (2003) 299.

[183] N. Tsuboi, Y. Takahashi, S. Kobayashi, H. Shimizu, K. Kato, F. Kaneko, J. Phys. Chem. Solids 64 (2003) 1671.

[184a] A.N. Banerjee, R. Maity, K.K. Chattopadhyay, Mater. Lett. 58 (2003) 10.

[184b] A.N. Banerjee, C.K. Ghosh, S. Das, K.K. Chattopahyay, Physica B, in press.

[185] Y. Wang, H. Gong, Adv. Mater. CVD 6 (2000) 285.

[186] H. Gong, Y. Wang, Y. Luo, Appl. Phys. Lett. 76 (2000) 3959.

[187] Y. Wang, H. Gong, F. Zhu, L. Liu, L. Huang, A.C.H. Huan, Mater. Sci. Eng. B 85 (2001) 131.

[188] H. Ohta, K. Nomura, M. Orita, M. Hirano, K. Ueda, T. Suzuki, Y. Ikuhara, H. Hosono, Adv. Funct. Mater. 13 (2003) 139.

[189] H. Ohta, K. Nomura, M. Orita, M. Hirano, K. Ueda, T. Suzuki, Y. Ikuhara, H. Hosono, Thin Solid Films 411 (2002) 147.

[190] H. Hiramatsu, K. Ueda, H. Ohta, M. Orita, M. Hirano, H. Hosono, Appl. Phys. Lett. 81 (2002) 598.

[191] E. Bobeico, F. Varsano, C. Minarini, F. Roca, Thin Solid Films 444 (2003) 70.

[192] L. Dloczik, Y. Tomm, R. Könenkamp, Thin Solid Films 451−452 (2004) 116.

[193] H.K. Yoshida, T. Koyanagi, H. Funashima, H. Harima, A. Yanase, Solid State Commun. 126 (2003) 135.

[194] T. Koyanagi, H. Harima, A. Yanase, H.K. Yoshida, J. Phys. Chem. Solids 64 (2003) 1443.

[195] V. Patrick, G. Gavalas, J. Am. Ceram. Soc. 73 (1990) 358.

[196] C. Macricilly, P. Courty, B. Delmon, J. Am. Ceram. Soc. 53 (1970) 56.

[197] K. Tonooka, K. Shimokawa, O. Nishimura, Thin Solid Films 411 (2002) 129.

[198] D. Panda, P.K. Ghosh, A.N. Banerjee, R. Maity, K.K. Chattopadhyay, communicated.

[199] A. Kudo, H. Yanagi, K. Ueda, H. Hosono, H. Kawazoe, Y. Yano, Appl. Phys. Lett. 75 (1999) 2851.

[200] H. Ohta, K. Kawamura, M. Orita, N. Sarukura, M. Hirano, H. Hosono, Electron. Lett. 36 (2000) 984.

[201] H. Ohta, K. Kawamura, M. Orita, M. Hirano, N. Sarukura, H. Hosono, Appl. Phys. Lett. 77 (2000) 475.

[202] H. Ohta, M. Orita, M. Hirano, J. Appl. Phys. 89 (2001) 5720.

[203] H. Hosono, H. Ohta, K. Hayashi, M. Orita, M. Hirano, J. Cryst. Growth 237−239 (2002) 496.

[204] R.L. Hoffman, J.F. Wager, M.K. Jayaraj, J. Tate, J. Appl. Phys. 90 (2001) 5763.

[205] M.K. Jayaraj, A.D. Draeseke, J. Tate, R.L. Hoffman, J.F. Wager, Mat. Res. Soc. Proc. 666 (2001) F4.1.

[206] K. Tonooka, H. Bando, Y. Aiura, Thin Solid Films 445 (2003) 327.

[207] D.-K. Hwang, K.-H. Bang, M.-C. Jeong, J.-M. Myong, J. Cryst. Growth 254 (2003) 449.

[208] S. Tüzemen, G. Xiong, J. Wilkinson, B. Mischuck, K.B. Ucer, R.T. Williams, Physica B 308−310 (2003) 1197.

[209] T. Aoki, Y. Hatanaka, D.C. Look, Appl. Phys. Lett. 76 (2000) 3257.

[210] T.V. Butkhuzi, A.V. Bureyev, A.N. Georgobiani, N.P. Kekelidze, T.G. Khulordava, J. Cryst. Growth 117 (1992) 366.

[211] J.F. Wager, Science 300 (2003) 1245.

[212] M.W.J. Prins, K.-O. Grosse-Holz, G. Müller, J.F.M. Cillessen, J.B. Giesbers, R.P. Weening, R.M. Wolf, Appl. Phys. Lett. 68 (1996) 3650.

[213] M.W.J. Prins, S.E. Zinnemers, J.F.M. Cillessen, J.B. Giesbers, Appl. Phys. Lett. 70 (1997) 458.

[214] R.L. Hoffman, B.J. Norris, J.F. Wager, Appl. Phys. Lett. 82 (2003) 733.

[215] Satoshi Masuda, Ken Kitamura, Yoshihiro Okumura, Shigehiro Miyatake, Hitoshi Tabata, Tomoji Kawai, J. Appl. Phys. 93 (2003) 1624.

[216] P.F. Carcia, R.S. McLean, M.H. Reilly, G. Nunes Jr., Appl. Phys. Lett. 82 (2003) 1117.

[217] K. Nomura, H. Ohta, K. Ueda, T. Kamiya, M. Hirano, H. Hosono, Science 300 (2003) 1269.

[218] H. Ohta, K. Nomura, H. Hiramatsu, K. Ueda, T. Kamiya, M. Hirano, H. Hosono, Solid-State Electron. 47 (2003) 2261.
[219] A.L. Efros, A.L. Efros, Sov. Phys. Semicond. 16 (1982) 772.
[220] L.E. Brus, J. Chem. Phys. 80 (1984) 4403.
[221] A.J. Cox, J.G. Louderback, L.A. Bloomfield, Phys. Rev. Lett. 71 (1993) 923.
[222] A.P. Alivisatos, Science 271 (1996) 933.
[223] J.R. Heath, Science 270 (1995) 1315.
[224] T. Demel, D. Heitmann, P. Grambow, K. Ploog, Phys. Rev. Lett. 64 (1990) 2559.
[225] Q. Li, C. Wang, Appl. Phys. Lett. 83 (2003) 359.
[226] T. Demel, D. Heitmann, P. Grambow, K. Ploog, Phys. Rev. Lett. 66 (1991) 2657.
[227] D.L. Klein, R. Roth, A.K.L. Lim, A.P. Alivisatos, P.L. McEuen, Nature 389 (1997) 699.
[228] D.L. Feldheim, C.D. Keating, Chem. Soc. Rev. 28 (1998) 1.
[229] A.N. Banerjee, K.K. Chattopadhyay, J. Appl. Phys. 97 (2005) 084308.

Dr. K.K. Chattopadhyay is a Reader in the Department of Physics, Jadavpur University, Kolkata, India. He is also the Jt. Director of School of Materials Science and Technology and Jt. coordinator of the Nanoscience and Technology Center of Jadavpur University. Born in the year 1963, West Bengal, India, he had taken his Masters in Physics from the University of Calcutta and Ph.D. from Jadavpur University in 1993. He has done his post-doctoral work in the National Institute of Materials Science (NIMS), Japan. His current field of research interest includes p-type transparent conducting metal oxides, transparent electronics, and also various kinds of nanostructured materials and their applications.

Dr. Chattopadhyay has nearly 100 publications of research papers in different international journals of repute and also published a large number of papers in the proceedings of international conferences. He is the recipient of various awards and scholarships including Japan Society for Promotion of Science (JSPS), Centre of Excellence (COE), Government of Japan. He was a visiting professor at Hanyang University, South Korea. He is the life member of many academic bodies like Materials Research Society of India (MRSI).

Dr. A.N. Banerjee is currently doing his post-doctoral research as a Visiting Research Associate in the Nanoscale Device Research, Department of Electrical & Computer Engineering, University of Nevada, Las Vegas, USA.

Born in 1975, in Kolkata, India, he had done his Masters in Physics in 1999 from University of Calcutta, India and Ph.D. in the year 2005 from Jadavpur University, Kolkata, India on Thin Film Technology. His topic of research was syntheses and characterization of various transparent p-type semiconducting oxide thin films and fabrication of transparent junctions from them for possible applications in the field of "Transparent Electronics". His scientific interests also focused on the fabrication of different complex II−VI semiconductor nanostructures for possible applications in nanodevices such as nanoscale detectors, nanosensors, field-emitters etc. He is the recipient of the Senior Research Fellowship offered by the Scientific and Industrial Research, Government of India. He has more than 20 scientific publications in various journals and conference proceedings of international repute in his credit during his Ph.D. research work.

Dr. Banerjee is the member of several academic societies that include Indian Physical Society, Materials Research Society of India and Electron Microscopy Society of India. His current activities include the development of nanostructured p-type transparent conducting oxides and fabrication of nanoactive devices from them, nanostructure based corrosion-barrier coatings on steel and various substrates for transmutation applications, development of corrosion-resistance coatings on carbon nanotubes for field-emission applications, growth of metal/semiconductor quantum-dots and anti-dots as well as nanowires/rods and fabrication of diverse nanodevices from them.

Dr. Banerjee's website is: http://www.ee.unlv.edu/∼arghya/.